JOC The Journal of Organic Chemistry

Article

pubs.acs.org/joc

Combined Experimental and Computational Investigations of Rhodium- and Ruthenium-Catalyzed C−H Functionalization of Pyrazoles with Alkynes

Andrés G. Algarra,[†] Warren B. Cross,*[,‡,§] David L. Davies,*[,‡] Qudsia Khamker,[‡] Stuart A. Macgregor,*[,†] Claire L. McMullin,[†] and Kuldip Singh[‡]

[†]Institute of Chemical Sciences, Heriot-Watt University, Edinburgh EH14 4AS, U.K.

[‡]Department of Chemistry, University of Leicester, University Road, Leicester LE1 7RH, U.K.

Supporting Information

ABSTRACT: Detailed experimental and computational studies are reported on the mechanism of the coupling of alkynes with 3-arylpyrazoles at $[Rh(MeCN)_3Cp^*][PF_6]_2$ and $[RuCl_2(p\text{-cymene})]_2$ catalysts. Density functional theory (DFT) calculations indicate a mechanism involving sequential N−H and C−H bond activation, HOAc/alkyne exchange, migratory insertion, and C−N reductive coupling. For rhodium, C−H bond activation is a two-step process comprising κ^2−κ^1 displacement of acetate to give an agostic intermediate which then undergoes C−H bond cleavage via proton transfer to acetate. For the reaction of 3-phenyl-5-methylpyrazole with 4-octyne k_H/k_D = 2.7 ± 0.5 indicating that C−H bond cleavage is rate limiting in this case. However, H/D exchange studies, both with and without added alkyne, suggest that the migratory insertion transition state is close in energy to that for C−H bond cleavage. In order to model this result correctly, the DFT calculations must employ the full experimental system and include a treatment of dispersion effects. A significantly higher overall barrier to catalysis is computed at {Ru(*p*-cymene)} for which the rate-limiting process remains C−H activation. However, this is now a one-step process corresponding to the κ^2−κ^1 displacement of acetate and so is still consistent with the lack of a significant experimental isotope effect (k_H/k_D = 1.1 ± 0.2).

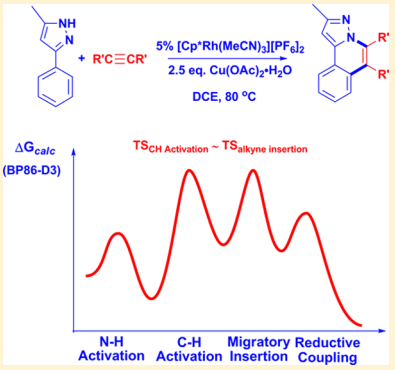

INTRODUCTION

Metal-catalyzed C−H functionalization has become a focus for research for more atom-efficient methods for construction of C−C and C−E bonds (E = O, N).[1] These methods avoid the requirement to prefunctionalize the C−H bond, usually to a C−X bond (X = Cl, Br, I), and avoid the formation of salt waste in the subsequent C−C or C−E bond formation reaction. In particular, the recognition by us[2] and others[3] of the role of carboxylates in providing facile C−H activation has led to a huge upsurge in interest in this field. We have characterized this as ambiphilic metal−ligand assisted (AMLA)[2d,e] C−H activation, reflecting the synergic role of both metal center and intramolecular carboxylate base in promoting this process, and this is closely related to the concerted metalation−deprotonation (CMD) concept proposed by Fagnou and co-workers.[3f] This increased understanding of the mechanism of this C−H activation process has enhanced its use in catalysis.

The use of Rh(III) catalysts based on $[RhCl_2Cp^*]_2$ and related derivatives for C−H functionalization was pioneered by the groups of Miura[4] and Fagnou.[5] However there has been a huge increase in interest in the past few years and the field has recently been reviewed.[6] This methodology has allowed access to substituted naphthalenes and to a wide range of heterocycles. More recently, related chemistry has been demonstrated using $[RuCl_2(p\text{-cymene})]_2$ as the catalyst precursor.[1f,7]

It has been noted for rhodium catalysts that neutral directing groups undergo 1:2 coupling with alkynes to give naphthalenes; in contrast, substrates that contain a protic E−H (E = N, O) directing group can undergo deprotonation (E−H activation) and typically undergo 1:1 coupling with alkynes and give heterocyclic products.[6] With benzamides, both possibilities have been observed depending on the substitution pattern (see Scheme 1). We have become interested in directing groups that can have an NH group through tautomerisation and can then potentially react by either pathway.

A general catalytic cycle proposed for heterocycle formation is shown in Scheme 2. Opening of the dimer precursor in the presence of $Cu(OAc)_2$ gives a $[M(OAc)_2(ring)]$ intermediate (**A**), which can effect N−H and C−H bond activation of the

Scheme 1

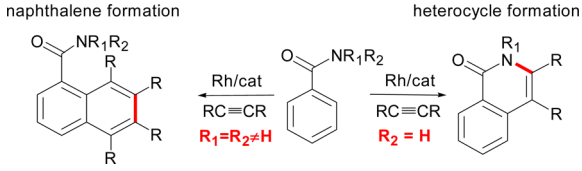

Received: November 22, 2013
Published: February 24, 2014

Scheme 2

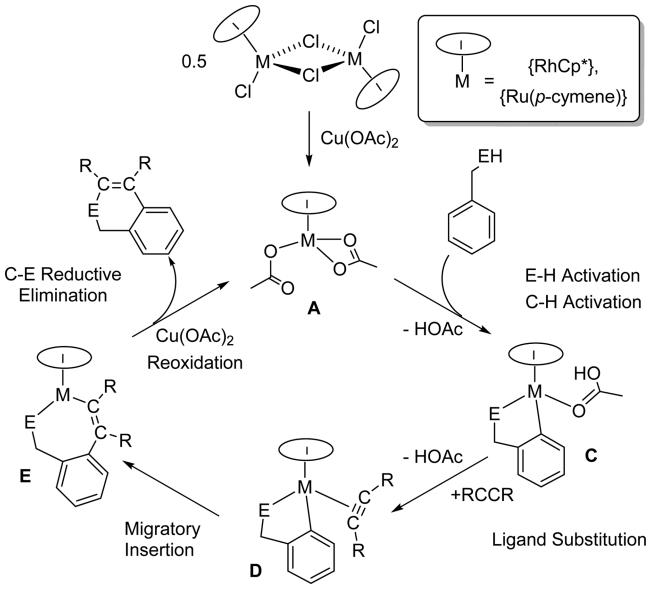

substrate to form a 5-membered metallacycle (**C**). After HOAc/alkyne substitution, migratory insertion gives a 7-membered metallacycle (**E**) from which reductive elimination with C−E bond formation gives the heterocyclic product. The Rh(I) or Ru(0) species formed in this step is reoxidized in the presence of $Cu(OAc)_2$ to regenerate the $[M(OAc)_2(ring)]$ active species.

Direct evidence for some of the steps in Scheme 2 has been obtained from the observation of stoichiometric C−H activation at complexes based on {RhCp*},[8] as well as in some cases for the subsequent alkyne insertion.[8a,e,9] Such studies have usually employed neutral directing groups, although the first examples of intermediates formed from anionic directing groups have recently also been isolated.[10] However, mechanistic information on the catalytic reactions is hampered by the difficulty in isolating intermediates, meaning that information on the relative accessability of the different steps is difficult to establish. Deuteration studies can show whether C−H activation is reversible. In addition, while kinetic isotope effects (k_H/k_D) can in principle give information on whether C−H activation is the rate-limiting step in catalysis, Hartwig[11] has recently highlighted the difficulties in correctly interpreting such data.

One additional means to gain mechanistic insight is the use of density functional theory (DFT) calculations to complement experimental observations. To date, only two DFT studies on heterocycle formation via {RhCp*}-catalyzed C−H functionalization have been published, both of which focused on benzamide derivatives, ArC(O)NH(OR), in which the N-bound OR group acts as an internal oxidant.[12] In their computational study, Guimond et al. considered isoquinolone formation via the reaction of PhC(O)NH(OAc) with acetylene at a simple $Rh(OAc)_2Cp$ model catalyst.[13] More recently Xia and co-workers revisited this system for dihydroquinolone formation via coupling of PhC(O)NH(OR) (R = Me, C(O)tBu) and ethene at $Rh(OAc)_2Cp^*$.[14] Both studies propose that the highest lying transition state in the overall process corresponds to the C−H activation step, and Guimond et al. interpreted this as being consistent with the significant k_H/k_D kinetic isotope effect (15 ± 1) observed experimentally for the $[RhCl_2Cp^*]_2$-catalyzed reaction of C_6H_5/D_5-C(O)NH-(O_2C^tBu) with MeCCPh. In contrast, the closely related PhC(O)NH(OMe) substrate gave no k_H/k_D kinetic isotope effect, suggesting that the nature of the rate-limiting transition state changes with the identity of the internal oxidant. No calculations on the PhC(O)NH(OMe) process were reported.

Here we report synthetic and mechanistic studies on the highly efficient C−H functionalization of 3-phenylpyrazoles with alkynes at a {RhCp*} center and show similar reactivity at {Ru(*p*-cymene)}. In contrast to *N*-phenylpyrazole which gives naphthalenes,[15] the presence of an NH proton which can be deprotonated leads to formation of heterocyclic pyrazoloisoquinoline products. In particular, for rhodium catalysis we have extended the range of alkynes as coupling partners and shown that $[Rh(MeCN)_3Cp^*][PF_6]_2$ is a more efficient catalyst precursor than $[RhCl_2Cp^*]_2$. In addition, we demonstrate that for both rhodium and ruthenium the reactions can be run using catalytic rather than stoichiometric copper as the reoxidant. Deuteration and competition experiments, coupled

Table 1. Catalyst Optimization

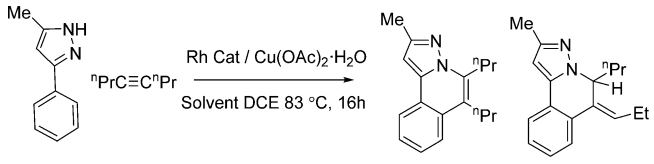

1a 2a 3aa 4aa

	catalyst	mol %	$Cu(OAc)_2$ (equiv)	yield of **3aa**[a] (%)
1	$[RhCl_2Cp^*]_2$	5	2.5	9
2	$[Rh(MeCN)_3Cp^*][PF_6]_2$	5	2.5	98
3	$[Rh(MeCN)_3Cp^*][PF_6]_2$	0	2.5	0
4	$[Rh(MeCN)_3Cp^*][PF_6]_2$	5	0	5[b,c]
5	$[Rh(MeCN)_3Cp^*][PF_6]_2$	1	2.5	8[b]
6[d]	$[RuCl_2(p\text{-cymene})]_2$	5	2.5	65
7	$[Rh(MeCN)_3Cp^*][PF_6]_2$	5	0.1	50 + 24% of **4aa**
8	$[RuCl_2(p\text{-cymene})]_2$	5	0.1	48
9	$[RuCl_2(p\text{-cymene})]_2$[e]	5	0.1	70

[a]Isolated yield after chromatography. [b]NMR yield after 17 h, using internal standard. [c]Yield increased to >95% after addition of 2.5 equiv of $Cu(OAc)_2$. [d]In *t*-AmOH 120 °C. [e]20 mol % of $AgPF_6$ additive.

dx.doi.org/10.1021/jo402592z | J. Org. Chem. 2014, 79, 1954−1970

Scheme 3. Scope of C−H Functionalization of Pyrazoles with Alkynes[a]

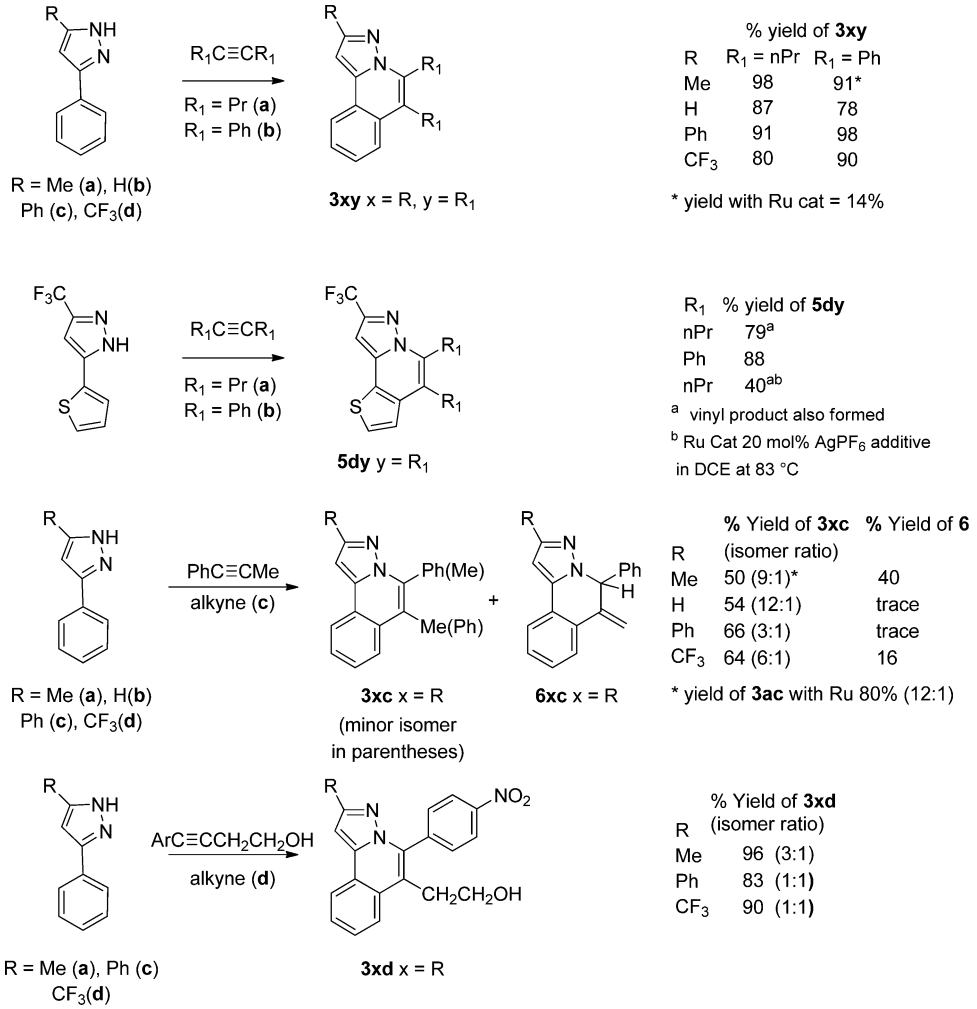

[a]Standard conditions: 2.5 equiv of $Cu(OAc)_2 \cdot H_2O$ with 5 mol % of catalyst, either $[Rh(MeCN)_3Cp^*][PF_6]_2$ in DCE at 83 °C or $[RuCl_2(p\text{-cymene})]_2$ in *t*-AmOH at 120 °C.

with detailed DFT calculations, have provided a detailed understanding of the mechanism of the catalysis and suggest that while C−H activation is rate limiting, the subsequent reaction with alkynes can be competitive with this process. The computational results stress the importance of employing an appropriate model in the calculations as well as including a treatment of dispersion effects. In addition, the calculations show that even if C−H activation is involved in the rate determining process, it does not follow that a k_H/k_D KIE will necessarily be observed. During the course of our work some related chemistry using $[RhCl_2Cp^*]_2$ as catalyst was reported by Li[16] for arylalkynes and similar reactions catalyzed by $[RuCl_2(p\text{-cymene})]_2$ were subsequently reported by Ackermann.[17]

RESULTS AND DISCUSSION

Catalytic Studies. Initially, we examined the reaction of 3-phenyl-5-methylpyrazole (**1a**) with 4-octyne using different catalysts and reaction conditions (Table 1). It is clear that $[Rh(MeCN)_3Cp^*][PF_6]_2$ (entry 2) is a much better catalyst than $[RhCl_2Cp^*]_2$ (entry 1), forming heterocycle **3aa** in quantitative yield. We confirmed that there was no catalysis in the absence of rhodium (entry 3). In the absence of $Cu(OAc)_2$ (entry 4) we observed a 5% yield of **3aa**, i.e., stoichiometric based on the amount of $[Rh(MeCN)_3Cp^*][PF_6]_2$ catalyst, indicating that reductive elimination can occur without prior oxidation. Lowering the catalyst loading to 1 mol % led to very low conversions. For comparison, all reactions were left overnight to go to completion; however, detailed reaction monitoring showed that when $[Rh(MeCN)_3Cp^*][PF_6]_2$ was used as catalyst the reaction was complete in 1 h at 83 °C. We also tested $[RuCl_2(p\text{-cymene})]_2$ as a catalyst precursor, and this also gave **3aa** in good (65%) yield, athough under somewhat harsher conditions than rhodium. Moreover, unlike related reactions recently reported by Ackermann,[17] for **3aa** we found no need to use Ag^+ salts as additives. Finally, we tested both catalysts with only catalytic copper, using air as the external oxidant. Using rhodium (entry 7), the yield of **3aa** was reduced (50%) and importantly, a new isomeric product **4aa** was also formed (24%). Similarly with ruthenium (entry 8) the yield with catalytic copper was slightly reduced (48%). However, addition of 20 mol % of $AgPF_6$ to give a cationic catalyst resulted in a 70% yield even with catalytic copper, and no **4aa** was observed (entry 9). Hence, we have demonstrated that both these catalytic systems can work with only catalytic copper using air as the external oxidant thus improving the overall efficiency of the process.

dx.doi.org/10.1021/jo402592z | J. Org. Chem. 2014, 79, 1954−1970

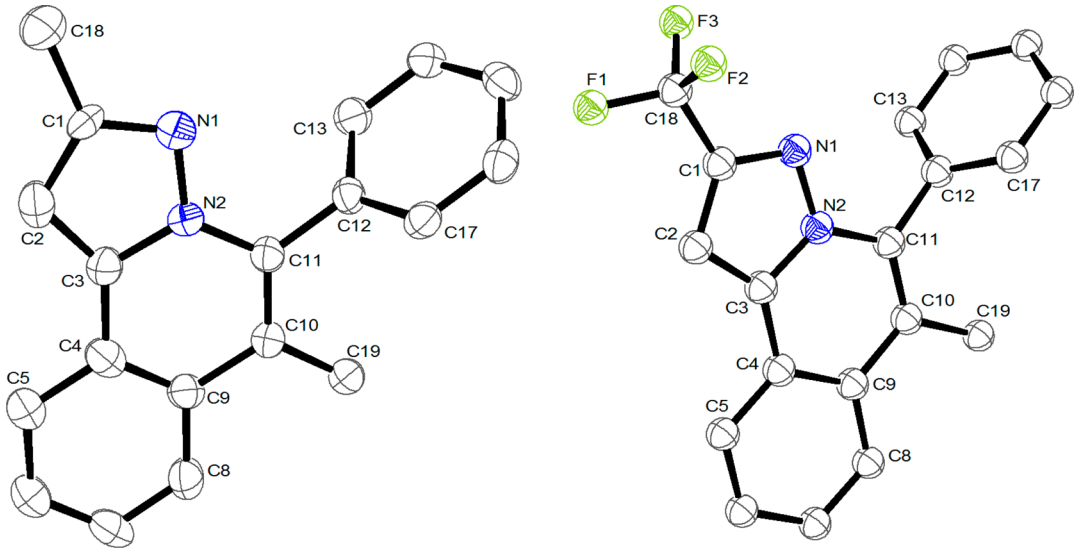

Figure 1. ORTEP plots of **3ac** (left) and **3dc** (right). Thermal ellipsoids are drawn at 50% probability and hydrogen atoms are omitted for clarity.

Since in the case of rhodium using catalytic copper led to some isomeric products, we explored the effects of using stoichiometric copper on the reactivity scope for rhodium and selected examples for ruthenium catalysis (see Scheme 3). Changing the substituent on the pyrazole had little effect, with good yields of **3ba**, **3ca**, and **3da** being formed in reactions with 4-octyne. Next, we tried diphenylacetylene, which gave products **3ab**−**db** in high yields. During the course of this work, Li et al. reported formation of **3ab**−**cb** in broadly similar yields.[16] However, they noted reduced yields with electron-withdrawing CF_3 on the pyrazole and difficulty in activating heterocyclic C−H bonds. In contrast, using $[Rh(MeCN)_3Cp^*][PF_6]_2$ as catalyst with a CF_3-substituted pyrazole we obtained **3db** in 90% yield. Indeed, even substrates which require C−H activation of a thiophene work well with a CF_3-substituted pyrazole, giving **5da** and **5db**, in 79 and 88% yields, respectively. The results with ruthenium were less consistent. Thus, though the product with 4-octyne, **3aa**, was formed in good yield (65% Table 1 entry 6) the corresponding product from diphenylacetylene, **3ab**, was only formed in 14% yield even in the presence of $AgPF_6$ as additive, while the thiophene substrate with a CF_3-substituted pyrazole with 4-octyne gave **5da** in 40% yield; in this case, addition of $AgPF_6$ was essential.

As both dialkyl- and diarylalkynes react to give heterocyclic products, we were interested in investigating the regioselectivity with a mixed aryl/alkylalkyne. Thus, PhC≡CMe (**2c**) reacted with **1a** to give **3ac** as a 9:1 ratio of isomers in 50% combined yield with 40% yield of isomer **6ac** (see below). The isomers of **3ac** could be separated by chromatography, and the major isomer is that shown, with the Ph substituent next to the N atom in the heterocycle. Interestingly, this reaction with a Ru catalyst gave 80% yield with a slightly higher selectivity of 12:1. This implies a preference for insertion with an aryl next to the metal and is consistent with previous studies of catalytic heterocycle synthesis from alkynes with RhCp* and Ru(p-cymene) catalysts.[18] Unsubstituted pyrazole **1b** reacted similarly to give **3bc** in 54% combined yield[19] as a 12:1 ratio of isomers. The phenyl- and trifluoromethyl-substituted phenylpyrazoles reacted similarly to form **3cc** and **3dc**, respectively, in good yields.

Similar reactions also occur with more functionalized alkyl groups. Thus, $R_1C{\equiv}CCH_2CH_2OH$ (**2d** R_1 = *p*-$C_6H_4NO_2$) reacted with **1a** and **1c** to give **3ad** and **3cd** in high yields. In both cases, two regioisomers were observed with the dominant product being that with the aryl substituent adjacent to N. However, there is significantly more of the minor isomer in these cases than for PhC≡CMe, the isomer ratio being 3:1 for **3ad** and 1:1 for **3cd** (compared to 9:1 and 3:1 for **3ac** and **3cc**, respectively). It is possible in these cases that in the minor isomer the hydroxyethyl side chain may be able to hydrogen bond to the uncoordinated nitrogen of the pyrazole, thereby leading to a relative stabilization of this isomer or an intermediate that leads to this isomer.

Several of the products have been characterized by X-ray crystallography. The structures of the major isomers of **3ac** and **3dc** are shown in Figure 1 and those of **3da**, **5da**, and **3db** are in the Supporting Information. The three fused rings are coplanar but are not completely delocalized. The central ring shows clear evidence of bond localization, as expected from Clar's rule,[20] with the original alkyne bond C(10)−C(11) now being a double bond (C=C = 1.36−1.38 Å) and the bond joining the phenyl or thiophene to the pyrazole being 1.43−1.44 Å. The structures of the major isomers of **3ac** and **3dc** confirm that the Ph substituent is on the carbon attached to nitrogen.

In the reaction of **1a** with **2a** in the presence of catalytic copper it is noticeable that a second isomeric product **4aa** is formed in addition to the normal heterocyclic product **3aa**. Similarly in some of the reactions with alkyne **2c** isomeric products **6** are also observed. Products arising by formal hydrogen shifts have been noticed in rhodium oxidative couplings previously,[21] and equivalent products have been realized through the use of allene coupling partners.[22] We have tested both products and find that they do not interconvert in either direction when exposed to the catalyst and oxidant under catalytic conditions. In principle, compounds **6** could arise from insertion of an allene that is itself formed by isomerization of PhC≡CMe; however our DFT calculations indicate that this route is not energetically feasible as the barrier to C(sp^3)−N reductive coupling step is prohibitively high in energy. A

dx.doi.org/10.1021/jo402592z | J. Org. Chem. 2014, 79, 1954−1970

Scheme 4

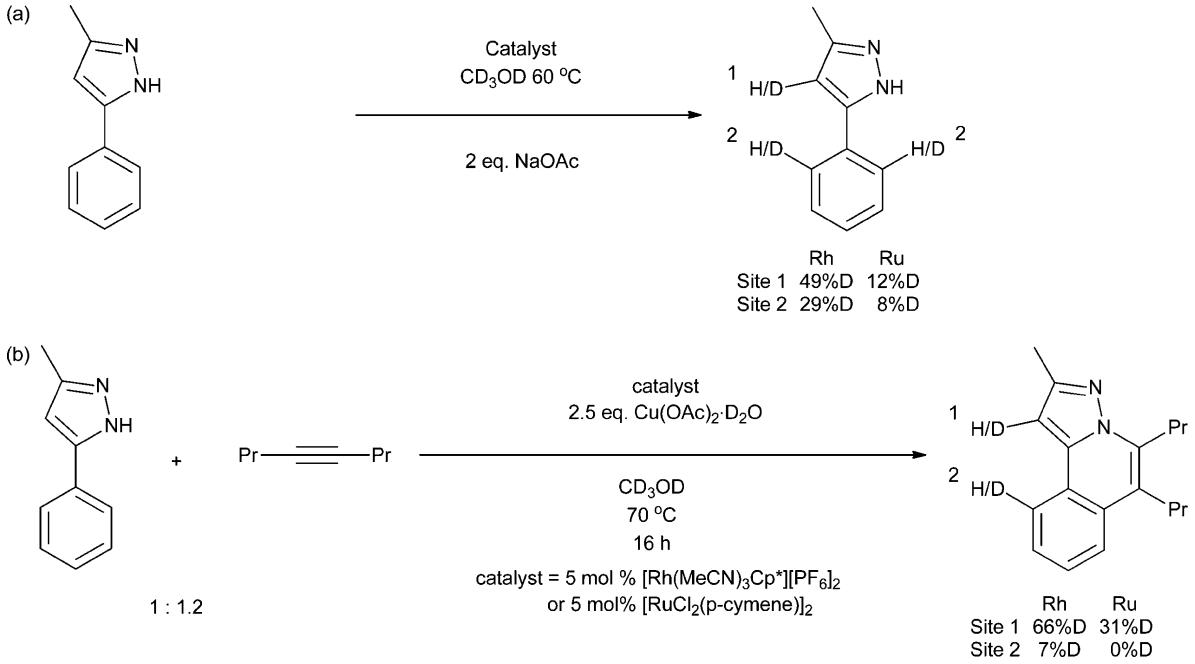

possible alternative mechanism is discussed in the computation section below.

In all these reactions, only heterocyclic products are formed, and there is no trace of naphthalene-type products which were formed from *N*-phenylpyrazole.[15] This outcome is therefore consistent with that shown in Scheme 2, i.e., N−H and C−H activation followed by alkyne insertion, C−N reductive coupling, and reoxidation of the catalyst.[23]

Experimental Mechanistic Studies. A series of experiments was conducted to shed light on the mechanism of catalysis at both Rh and Ru metal centers. With Rh, attempted stoichiometric cyclometalation of **1a** led to broad NMR spectra suggesting the presence of exchange processes. The reversibility of the C−H activation step was therefore assessed by a deuteration study. Treating substrate **1a** with $[Rh(MeCN)_3Cp^*][PF_6]_2$ (5 mol %) and 2 equiv of NaOAc in methanol-d_4 gave approximately 29% deuterium incorporation into each of the *ortho* positions after 16 h at 60 °C (see Scheme 4, a). Surprisingly, almost 50% deuterium exchange also occurred at the remaining pyrazole proton. We did consider whether this exchange may occur via a rollover cyclometalation, involving reprotonation at N and N-decoordination from cyclometalated intermediate **C**, rotation about the C1−Ph bond, and reversible C−H activation at the C4 pyrazole position. However, BP86-D3 calculations indicate that the double-cyclometalated species implicated in this pathway would be too high in energy (G_{DCE} = 22.0 kcal/mol) and so ruled out this mechanism (see the Supporting Information for details). Alternatively, it is possible that when the pyrazole is coordinated the C4 proton becomes more acidic and so can undergo exchange without direct involvement of the rhodium. Adding $Cu(OAc)_2$ had little effect, similar deuteration being observed. As has been observed previously[22] addition of d_1-pivalic acid increased the rate and extent of deuterium exchange. It is worth noting that to see deuterium incorporation into the substrate requires not only that N−H and C−H activation are reversible but also that exchange of free and bound pyrazole is facile under these conditions. If C−H activation is reversible but substrate exchange is not facile then only the bound substrate can undergo exchange (i.e., 5%, equivalent to the catalyst loading).

The deuteration experiment was repeated in the presence of a slight excess of alkyne and $Cu(OAc)_2$, i.e., similar to the catalytic conditions, although using methanol-d_4 as solvent in place of dichloroethane (see Scheme 4, b). In this case at only low conversion (<10%) the product showed no deuterium incorporation by NMR spectroscopy suggesting that the cyclometalated intermediate is being intercepted by the alkyne rather than going back to starting material. However, if the reaction is allowed to go to completion there is deuterium incorporation in both positions though considerably less at the *ortho* position (7%) compared to the pyrazole position (66%). Given that the alkyne is in slight excess (1.2 equiv), at high conversion the alkyne concentration is approximately 0.2 times that at the start; hence, at this stage the rate of H/D exchange in the *ortho* position (i.e., the reverse of C−H activation) is competitive with alkyne insertion. These observations suggest that the barriers to the forward (alkyne insertion) and reverse reactions (C−H activation) are similar in energy.

Similar experiments were carried out with ruthenium. In this case, in the absence of alkyne there was significantly less deuterium incorporation, suggesting that C−H activation is less reversible for ruthenium. As for rhodium, exchange at the pyrazole position occurred as well as at the *ortho* positions of the phenyl. However, in the presence of substrate ruthenium gave a different result; even at high conversion there was only deuterium incorporation into the pyrazole C4 position and no H/D exchange in the phenyl ring.[24] This suggests that in this case alkyne insertion is significantly easier than the reverse of C−H activation (see below). Note, the observation that deuterium exchange in the pyrazole position is less affected by alkyne than exchange in the phenyl positions is also consistent with pyrazole exchange not occurring via a rollover mechanism.

A value for k_H/k_D for rhodium was measured using **1a**-d_3 and was determined to be 2.7 ± 0.5 (see Scheme 5).[25] This suggests

dx.doi.org/10.1021/jo402592z | J. Org. Chem. 2014, 79, 1954−1970

Scheme 5. Parallel KIE Experiments

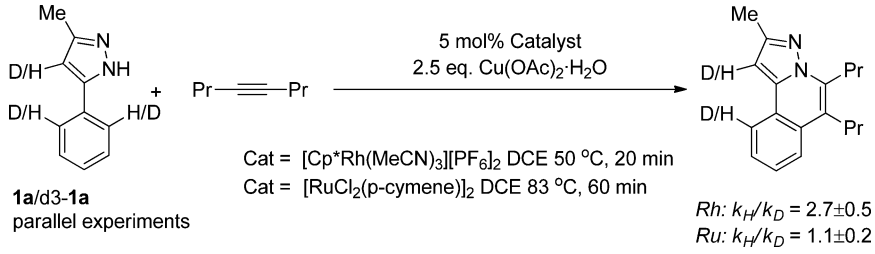

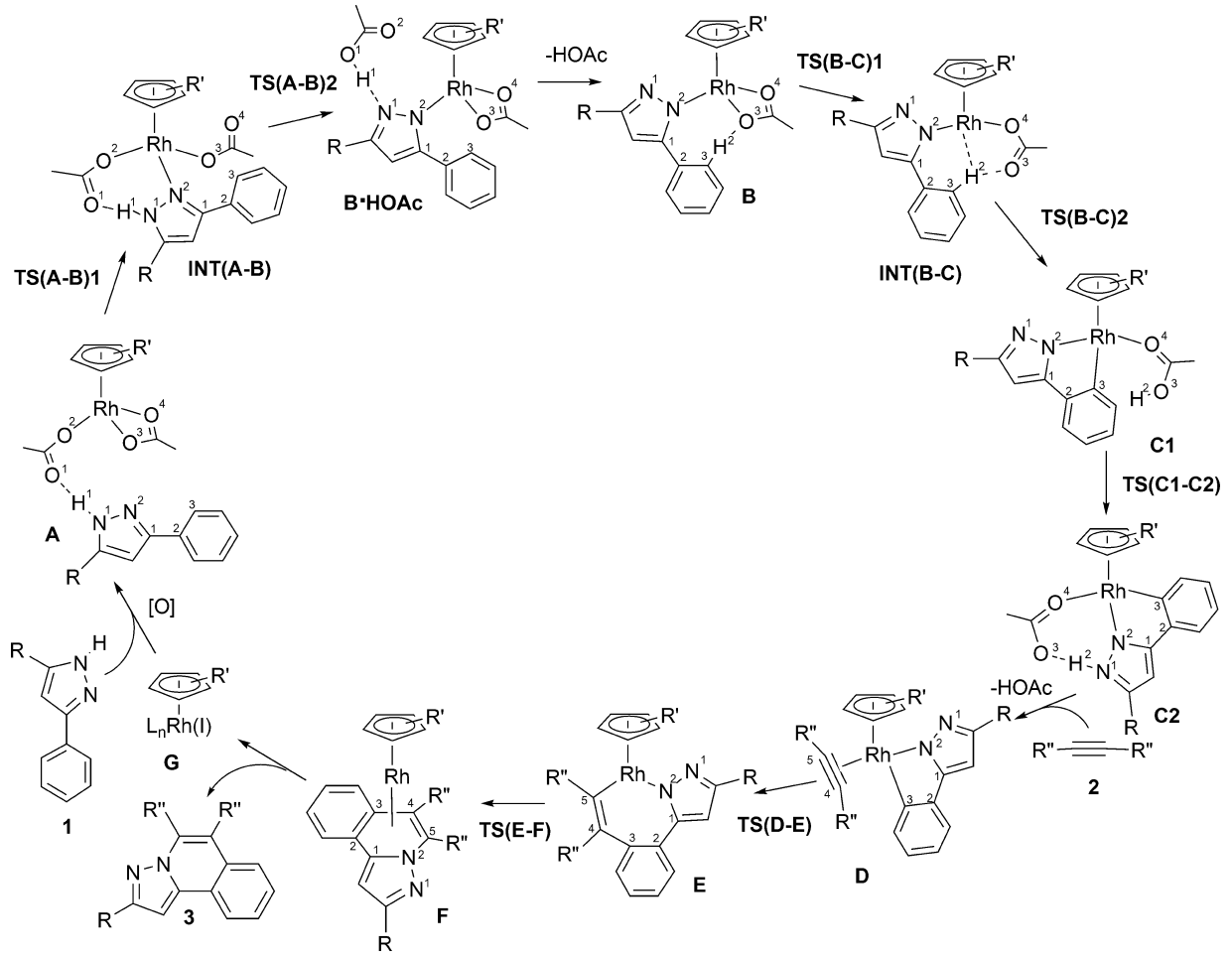

Figure 2. Mechanism for coupling of alkynes with 3-phenylpyrazoles at $Rh(OAc)_2(C_5R'_5)$ catalysts computed with model 1 (R = R′ = R″ = H) and model 2 (R = R′ = Me, R″ = ^{n}Pr).

that C−H bond cleavage is likely involved in the rate-determining step. To confirm this, the order of reaction with respect to alkyne was measured using initial rates, and this showed near zero order in alkyne (0.07 ± 0.1), again consistent with C−H bond cleavage being rate limiting. Similar deuteration and KIE studies were carried out for ruthenium. The k_H/k_D was determined to be 1.1 ± 0.2, and this could be interpreted as indicating that C−H bond activation is not rate determining; however, this reaction is also zero order in alkyne (0.0 ± 0.1). Our DFT calculations show that the rate-determining step in fact corresponds to the κ^2-κ^1 displacement of acetate that must occur as the first step of the C−H activation process prior to actual C−H bond cleavage (see below).

Computational Mechanistic Studies. Density functional theory calculations have been performed to assess the mechanism of the coupling of alkynes with 3-phenylpyrazoles at catalysts based on {RhCp*} and {Ru(*p*-cymene)} fragments. For the Rh system, two models have been employed: model 1, which combines simplified substrates and catalyst, i.e., 3-phenylpyrazole with HCCH and $Rh(OAc)_2Cp$, and model 2, which uses the actual substrates and catalyst used experimentally, i.e., 3-phenyl-5-methylpyrazole (**1a**), reacting with ^{n}PrCC^{n}Pr (**2a**) at $Rh(OAc)_2Cp^*$. All geometries have been optimized with the BP86 functional, and we report G_{DCE}, i.e., gas-phase free energies corrected for the effects of DCE solvent through the PCM approach. In a further step, a correction for dispersion effects (using Grimme's D3 parameter set) was added to the BP86 results, and a number of alternative density functionals were also tested. The calculations indicate that the same basic catalytic cycle is in operation for both models 1 and

dx.doi.org/10.1021/jo402592z | J. Org. Chem. 2014, 79, 1954−1970

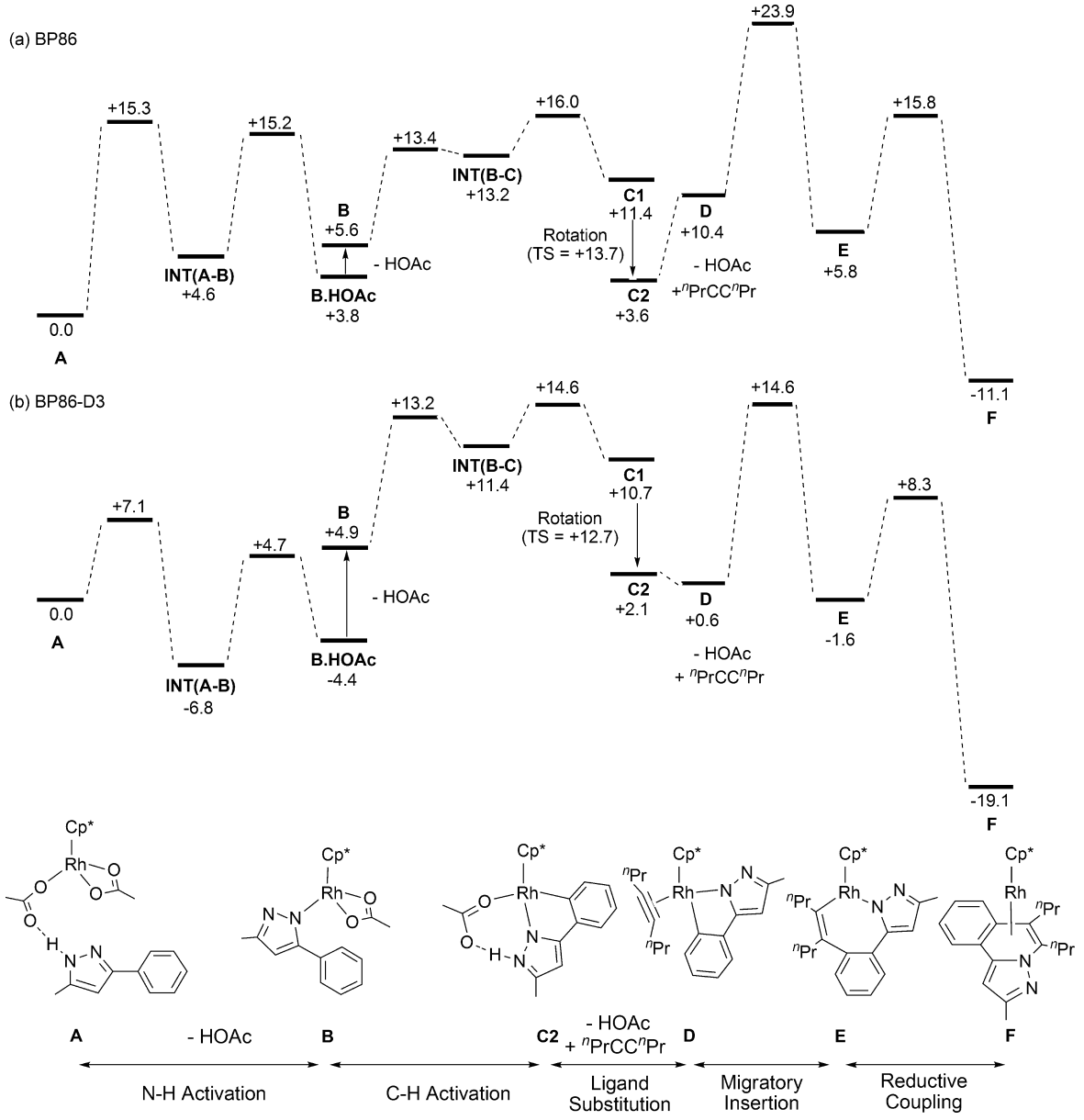

Figure 3. Computed reaction profiles (G_{DCE}, kcal/mol) for the coupling of ^{n}PrCC^{n}Pr with **1a** at Rh(OAc)$_2$Cp* (model 2): (a) BP86 functional; (b) BP86-D3.

2, but that the reaction energetics vary considerably with the model and functional adopted. In particular, we show how the use of an oversimplified model such as model 1 is inappropriate if a detailed modeling of the catalysis is to be achieved. In the following we therefore first describe the overall mechanism and then discuss the computed energetics in the light of the available experimental data. Computed geometries are generally standard and are supplied in full in the Supporting Information, with only selected key structures being highlighted for more detailed discussion.

The catalytic cycle computed for both models 1 and 2 starts with adduct **A**, in which the pyrazole substrate **1** is H-bonded to the pendant oxygen of the κ^1-acetate ligand in Rh(OAc)$_2$(C$_5$R′$_5$) (see Figure 2, which also gives the atom labeling scheme employed). For model 2, this H-bonded adduct is computed to be 2.8 kcal/mol more stable than the separated reactants. N−H activation in **A** proceeds in two steps, first, formation of the Rh−N^2 bond (with κ^2- κ^1 displacement of the second acetate ligand) to give **INT(A-B)**, followed by N^1−H^1 bond cleavage induced by acetate dissociation via elongation of the Rh−O^2 bond. This forms **B·HOAc** in which acetic acid is H-bonded to N^1 and the spectator acetate has reverted to a κ^2-binding mode. Loss of HOAc then gives **B**, which can undergo C−H activation via an agostic intermediate, **INT(B−C)**, formed via κ^2−κ^1 displacement of acetate by the approaching *ortho*-C−H bond of the substrate. This allows for intramolecular H−bonding to acetate, which promotes C−H bond cleavage via **TS(B−C)2**. Together, these two steps comprise an AMLA/CMD C−H bond activation.[2d,3f] The cyclometalated intermediate **C1** is initially formed from which a more stable form, **C2**, can be readily accessed via rotation about the Rh−O^4 bond. HOAc/alkyne exchange then forms **D**, which undergoes migratory insertion (**D**→**E**) followed by C−N reductive coupling to give **F** in which the pyrazoloisoquinoline product, **3**, is η^4-bound to the Rh center. Experimentally, this last step has been shown to occur in the absence of added Cu(OAc)$_2$

dx.doi.org/10.1021/jo402592z | J. Org. Chem. 2014, 79, 1954−1970

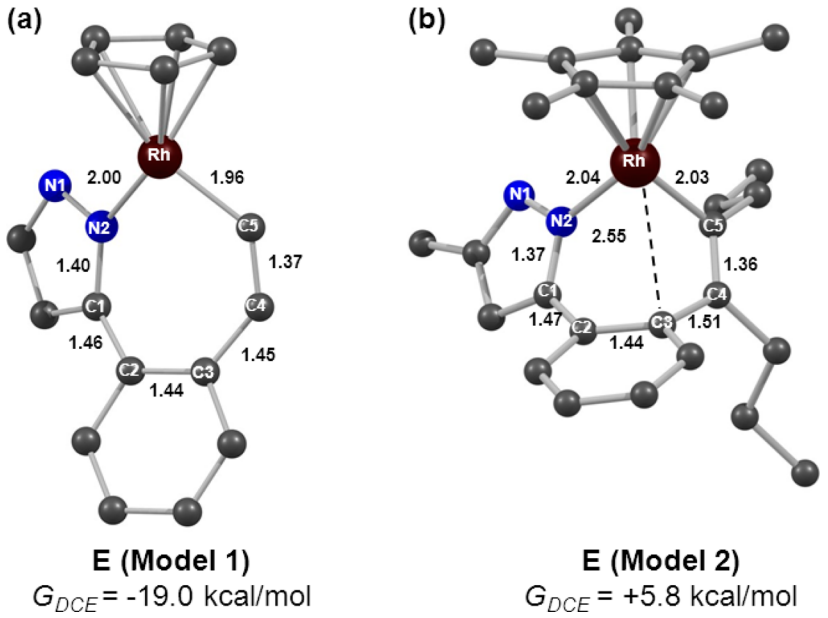

Figure 4. Computed structures of intermediate **E** for (a) model 1 and (b) model 2. Selected distances are given in angstroms and relative free energies in solution are in kcal/mol and are based on the BP86 functional. H atoms are omitted for clarity.

(see above) and so rules out any need for prior oxidation of the Rh center. The catalytic cycle is completed via release of **3** and reoxidation of an unspecified Rh(I) species, **G**, although we have not attempted to model these steps here.

Our initial results computed with model 1 show similar features to those computed by Guimond and co-workers for the reaction of PhC(O)NH(OAc) with HCCH at $Rh(OAc)_2Cp$ (see Figure C1 in the Supporting Information).[13] In the present case, N−H and C−H activation proceed with an overall barrier of 15.7 kcal/mol (corresponding to **TS(B−C)1**) to give cyclometalated **C2** at −2.4 kcal/mol. HOAc/HCCH exchange in **C2** then gives **D** at −1.0 kcal/mol from which migratory insertion proceeds via **TS(D-E)** at +9.8 kcal/mol to form **E** at −19.0 kcal/mol. C−N reductive coupling has a barrier of 16.5 kcal/mol and gives **F** at −35.0 kcal/mol. Comparing these computed results with experiment highlights some key discrepancies: (i) the formation of **C2** is computed to be exergonic, suggesting that a cyclometalated species should be observed in the absence of alkyne; however, this is not the case in the true experimental system; (ii) once **C2** is formed HOAc/alkyne substitution and migratory insertion is predicted to be far easier ($\Delta G^{\ddagger}_{DCE}$ = +12.2 kcal/mol) than the reverse C−H bond formation ($\Delta G^{\ddagger}_{DCE}$ = +18.1 kcal/mol); this is inconsistent with the persistence of H/D exchange in the presence of added alkyne.

These discrepancies associated with the small model led us to consider the full experimental system computationally (model 2, Figure 3a). The initial N−H and C−H activation steps are similar to those of model 1 and again have a small overall barrier (16.0 kcal/mol), although these processes are now endergonic (**C2**: G_{DCE} = +3.6 kcal/mol). The second half of the profile is more model-dependent, starting with a much less favorable HOAc/alkyne substitution (ΔG_{DCE} = +6.8 kcal/mol cf. +1.4 kcal/mol for model 1) that could be taken to reflect the greater bulk of model 2 (although see the discussion of dispersion effects below). **D** undergoes migratory insertion with a barrier of 13.5 kcal/mol, somewhat higher than model 1, although this step is now much less exergonic (ΔG_{DCE} = −4.6 kcal/mol cf. −18.0 kcal/mol). This reflects the different geometries of **E** computed with the two models (see Figure 4). In model 1, insertion of HCCH gives a near-planar 7-membered metallacycle that maximizes π-delocalization around the ring.[26] With 4-octyne the propyl substituents disfavor a planar arrangement, and instead, a boat-like conformation is seen. This also accounts for the lower barrier to C−N reductive coupling with model 2 ($\Delta G^{\ddagger}_{DCE}$ = 10.0 kcal/mol cf. 16.5 kcal/mol for model 1) as less distortion is required to access the boat-like conformation necessary for C−N bond formation in the transition state. The overall formation of **F** is also far less favorable with model 2 (ΔG_{DCE} = −11.1 kcal/mol), and a significant component of this arises from the reduced intrinsic stability of the pyrazoloisoquinoline product, which is estimated to be ca. 15 kcal/mol less stable than with model 1.[27]

While model 2 predicts reversible and endergonic N−H and C−H activation, the rate-determining transition state is now clearly identified with the alkyne insertion step. This is at odds with the reduction in the extent of H/D exchange at the 3-phenylpyrazole *ortho* positions in the presence of alkyne, as this should not be affected if a significantly larger barrier to alkyne insertion exists. Moreover, rate-limiting alkyne insertion is inconsistent with the near-zero order dependency on 4-octyne concentration and the k_H/k_D value of 2.7 ± 0.5. To investigate these issues, we considered a range of density functionals with a particular focus on the computed difference in energy between **TS(D−E)** and the highest point along the N−H and C−H activation steps. The key outcome is that the transition states for these processes only become close in energy when a treatment of dispersion effects is included, either directly in the functional (B97D, M06) or in the protocol (BP86-D3, i.e., adding a dispersion correction to the BP86-optimized results). For ease of comparison we focus on the BP86-D3 results (see Figure 3b). A number of papers have highlighted the importance of dispersion corrections when computing ligand dissociation or ligand-exchange energies at transition-metal complexes.[28] Given this, as expected, the effects of the dispersion correction are most significant in processes involving

dx.doi.org/10.1021/jo402592z | J. Org. Chem. 2014, 79, 1954−1970

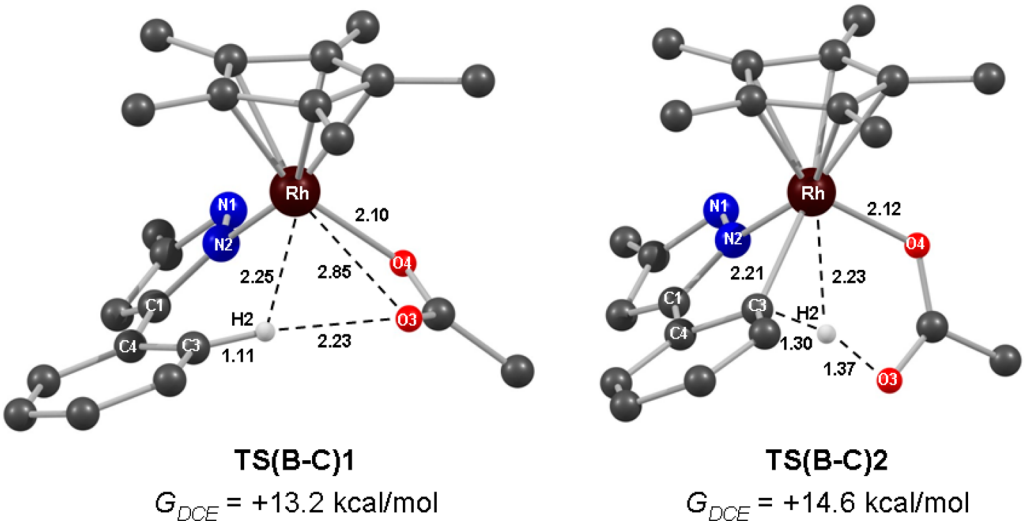

Figure 5. Computed structures of the AMLA/CMD C−H bond activation transition states, **TS(B−C)1** and **TS(B−C)2**, for model 2, with selected distances (Å) and relative free energies in solution (kcal/mol) at the BP86-D3 level. Spectator H atoms are omitted for clarity.

either ligand loss or substitution. Thus, **INT(A−B)** and the preceding transition state are both stabilized reflecting the movement of the 3-phenylpyrazole into the metal coordination sphere. Similarly, the loss of HOAc from **B·HOAc** is now more endergonic (+9.3 kcal/mol cf. +1.8 kcal/mol with the BP86 functional alone). The net result is that intermediate **B** and the subsequent stationary points associated with the intramolecular C−H activation are at similar relative energies with either BP86 or BP86-D3. A major effect is computed for the HOAc/4-octyne substitution (**C2** to **D**, BP86: ΔG_{DCE} = +6.8 kcal/mol; BP86-D3: ΔG_{DCE} = −1.5 kcal/mol). As the barrier to migratory insertion is similar with both approaches (ca. 14 kcal/mol), a significant stabilization of **TS(D-E)** is computed at the BP86-D3 level (G_{DCE} = +14.6 kcal/mol).[29]

In comparing the BP86-D3 profile with experiment, the stabilization of **INT(A−B)** means that the subsequent energetics must be quoted relative to this species. The formation of **C2** is now endergonic by +8.9 kcal/mol and has an increased barrier of 21.4 kcal/mol. H/D exchange is therefore reversible, with the equilibrium lying to the uncyclometalated reactants. Most importantly **TS(D−E)** (G_{DCE} = +14.6 kcal/mol) for alkyne insertion[29] is now at a similar energy to the N−H/C−H activation high point (**TS(B−C)2**, G_{DCE} = +14.6 kcal/mol): the two processes are therefore now competitive, more consistent with reduced *ortho*-H/D exchange in the presence of alkyne.[30] The overall barrier for the catalytic cycle is 21.4 kcal/mol. The BP86-D3 profile therefore captures much of the experimental behavior, with the transition states for C−H activation and alkyne insertion being very close in energy. We therefore propose the BP86-D3 protocol provides a robust approach to modeling the current system. Very similar behavior was computed with the M06 and B97D functionals, which also include a treatment of dispersion effects, although interestingly with M06L the alkyne insertion transition state remains 6.2 kcal/mol above that for C−H activation; at present we have no explanation for this behavior, although it appears to be linked to a less favorable energy for HOAc/4-octyne exchange (**C2→D**, ΔG = +10.5 kcal/mol) computed with this functional. A range of nondispersion corrected functionals (PBE, PBE0, BLYP, B3LYP) gave similar results to BP86, i.e., clearly (and incorrectly) suggesting rate-limiting alkyne insertion. As with BP86, the addition of the D3 dispersion correction to the PBE and PBE0 results again brought the free energies of **TS(B−C)2** and **TS(D−E)** to within 1 kcal/mol of each other. For BLYP and B3LYP, **TS(D−E)** is computed to lie approximately 14 kcal/mol above **TS(B−C)2** and although the dispersion correction reduces this to ca. 5 kcal/mol, alkyne insertion is still clearly identified as the rate-determining step. This, along with the rather high overall barriers computed with the BLYP-D3 and B3LYP-D3 approaches (in excess of 28 kcal/mol), suggest these functionals are a poor choice for the current system. Full details of all functional testing are given in the Supporting Information.

To interpret the observed k_H/k_D value of 2.7 ± 0.5 we have compared the computed geometries of the two transition states associated with the C−H bond activation process (see Figure 5). **TS(B−C)1** corresponds to the initial κ^2-κ^1 displacement of acetate by the incoming substrate, and as such, the C^3−H^2 bond is remote from the Rh center and shows little bond elongation (1.11 Å). In contrast, the transition state for C−H bond cleavage, **TS(B−C)2**, exhibits significant bond elongation (C^3···H^2 = 1.30 Å). In this case, as **TS(B−C)2** is higher in energy than **TS(B−C)1** it corresponds to the rate-determining transition state and the elongation of the C^3−H^2 bond is therefore consistent with the significant k_H/k_D value. Computation of the k_H/k_D KIE gives a value of 5.48, somewhat higher than the experimental figure, although it should be borne in mind that the latter will also include a contribution from the reverse reaction. However, more generally, our studies on AMLA/CMD C−H bond activation have shown the presence of both transition states is rather system-dependent and that in several cases only the initial κ^2−κ^1 acetate displacement transition state (equivalent to **TS(B−C)1**) is located.[2b,e] In such cases, the k_H/k_D value would be expected to be much closer to 1. Thus the nonobservation of a significant kinetic isotope effect may not necessarily mean that C−H bond activation can be ruled out as the rate-limiting step. Indeed, this appears to be the case for the {Ru(*p*-cymene)} system discussed below.

Reaction profiles have also been computed for the coupling of MeCCPh with pyrazole **1a** at $Rh(OAc)_2Cp^*$ (i.e., model 2) to probe the regioselectivity of this process. Similar profiles are

dx.doi.org/10.1021/jo402592z | J. Org. Chem. 2014, 79, 1954−1970

obtained to that computed for 4-octyne (see Table C3, Supporting Information), with the lower energy migratory insertion transition state, **TS(D−E)**, being computed when the Ph group is adjacent to the metal (G_{DCE} = 14.5 kcal/mol, 2.4 kcal/mol more stable than the alternative when Me is adjacent to the metal). Thus, the calculations correctly model the regioselectivity observed experimentally. A similar preference of 1.9 kcal/mol is also computed with the BP86 functional alone, indicating that dispersion effects and, hence, steric effects are not important in determining the regioselectivity. Instead, electronic effects dominate, and indeed a similar regioselectivity has been observed for alkyne insertion into 5-membered phosphanickelacycles.[31] In that case, DFT calculations linked this preference to the asymmetric distribution of the frontier molecular orbitals of MeCCPh, where both the π-bonding HOMO and π-antibonding LUMO have a greater contribution on the Me-substituted carbon. As both these orbitals participate in C−C bond fomation in the migratory insertion transition state this structure is therefore stabilized when the C(Me) center is involved in this process, i.e., when the Ph substitutent carbon is adjacent to the metal, as is the preference seen experimentally.

Another feature observed with MeCCPh is the formation of **6ac** as a significant side product. One possible route to this species would be via C(sp^3)−N reductive elimination from an intermediate such as $\mathbf{E2_{MePh}}$ (see Scheme 6), itself formed by

Scheme 6

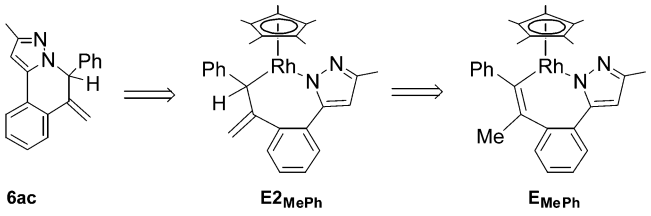

isomerization earlier in the cycle, for example from $\mathbf{E_{MePh}}$. However, the computed transition state barrier for this C(sp^3)−N bond formation is extremely high (+47.3 kcal/mol) and effectively rules out this possibility.

An analogous side product, **4aa**, was also seen with 4-octyne, and during the reaction screening it was noted that the proportion of this species increased when catalytic $Cu(OAc)_2$ was employed. This implies that side-product formation is enhanced when reoxidation of the Rh(I) species based on **F** is slow and, hence, that reorganization of **F** may be linked to side product formation. One such possible rearrangement is shown in Figure 6 and starts with slippage of the η^4-bound species $\mathbf{F_{MePh}}$ (G_{DCE} = −13.2 kcal/mol) formed upon C−N reductive coupling, to an η^2-bound species $\mathbf{F2_{MePh}}$ (G_{DCE} = −12.2 kcal/mol) where Rh interacts with the C^4−C^5 bond. $\mathbf{F2_{MePh}}$ also features an agostic interaction with one C^6−H bond and readily undergoes β-H transfer to give a hydrido allyl intermediate $\mathbf{F3_{MePh}}$ at −20.9 kcal/mol. H transfer back onto C^5 would generate $\mathbf{F4_{MePh}}$ from which **6ac** could dissociate; however, the high energy of $\mathbf{F4_{MePh}}$ (−4.9 kcal/mol) suggests this is unlikely. An alternative is that oxidation of $\mathbf{F3_{MePh}}$ can induce C−H reductive elimination, either with reformation of the C^6−H bond (to give **3ac**), or with C^5−H bond formation (to give **6ac**).

Having good agreement between experiment and computation for rhodium, we applied the same approach to ruthenium. The reaction profile computed at the BP86-D3 level for the coupling of pyrazole **1a** with 4-octyne at $Ru(OAc)_2$(*p*-cymene) is shown in Figure 7, where the solvent corrcetion has been performed with MeOH, reflecting the *t*-AmOH solvent used experimentally. The {Ru(*p*-cymeme)} system is observed to undergo slower H/D exchange in the absence of alkyne, and this is reflected in the computed barriers to both the forward C−H activation (25.4 kcal/mol) and the reverse process (16.9 kcal/mol), respectively 4.0 and 4.4 kcal/mol higher than for the {Cp*Rh} system. The major difference is the higher energy of **TS(B−C)1** (G_{DCE} = +16.8 kcal/mol). This corresponds to the κ^2−κ^1 acetate dissociation step and presumably reflects stronger Ru−OAc bonding in this case. Similarly, the energies of **TS(A-B)1** and **TS(A-B)2** are both ca. 4 kcal/mol higher than their {Cp*Rh} counterparts, and both of these also involve cleavage of an M−O bond. Once the agostic/H-bonded intermediate **INT(B−C)** is formed the subsequent C−H bond cleavage is barrierless on the G_{DCE} surface.[32]

From **C2**, HOAc/^{n}PrCC^{n}Pr substitution is slightly endergonic giving **D** at +2.3 kcal/mol. The subsequent migratory insertion has a somewhat lower barrier than at {Cp*Rh} (9.6 kcal/mol cf. 14.0 kcal/mol), and this, along with the facile reductive coupling, means that the C−H activation is clearly the

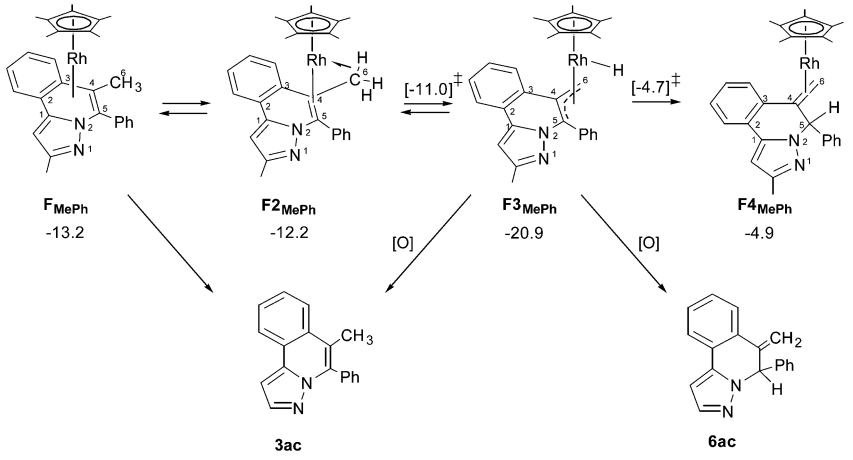

Figure 6. Possible mechanism of formation of isomerized heterocyclic product **6ac**. Relative free energies (G_{DCE}, kcal/mol) are computed with the BP86-D3 protocol.

dx.doi.org/10.1021/jo402592z | J. Org. Chem. 2014, 79, 1954−1970

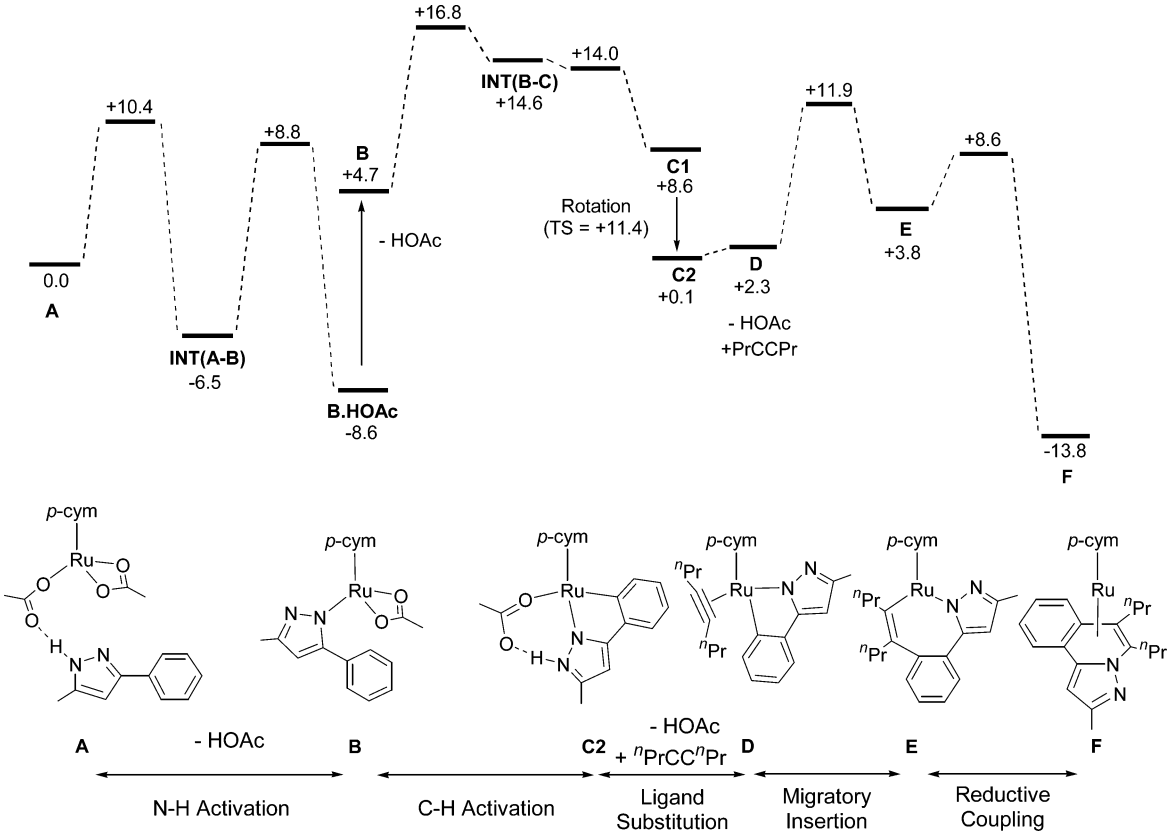

Figure 7. Computed reaction profiles (G_{MeOH}, kcal/mol) for the coupling of ^{n}PrCC^{n}Pr with **1a** at Ru(OAc)$_2$(*p*-cymene) (BP86-D3 protocol).

rate-limiting process in the Ru catalysis. The overall barrier for the coupling process is 25.4 kcal/mol, 4.0 kcal/mol higher than for Rh(OAc)$_2$Cp* and reflecting the harsher conditions required experimentally.[33] Moreover, the geometry of the rate-determining transition state, **TS(B−C)1**, is very similar to that computed at {RhCp*} in Figure 5 and so features minimal C−H bond elongation. Thus, despite the fact that the C−H bond activation process is rate-limiting, it does not follow that a significant k_H/k_D should be expected. Indeed, in agreement with this, the experimentally determined k_H/k_D is only 1.1 ± 0.2, while the calculated value is 1.23.

■ CONCLUSIONS

The Rh- and Ru-catalyzed formation of a range of pyrazoloisoquinolines has been demonstrated using a C−H functionalization strategy based on the coupling of 3-phenylpyrazoles with aryl- and alkylalkynes. For rhodium, [Rh(MeCN)$_3$Cp*][PF$_6$]$_2$ is shown to be a more effective precursor than [RhCl$_2$Cp*]$_2$ with efficient catalysis achieved at 80 °C. While catalysis with [RuCl$_2$(*p*-cymene)]$_2$ requires higher temperatures, for both metals the reactions can be run using catalytic rather than stoichiometric copper as the reoxidant. Deuteration and competition experiments on the rhodium catalysis suggest that C−H activation is reversible and rate limiting, but that the subsequent reaction with alkynes can be competitive with this process. For ruthenium, rate-limiting C−H bond activation is much less reversible and in the presence of alkyne is essentially irreversible.

DFT calculations on both rhodium and ruthenium catalysis indicate a mechanism involving sequential N−H and AMLA/CMD C−H bond activation, HOAc/alkyne exchange, migratory insertion, and C−N reductive coupling. Comparison of the computed energy profiles with the experimental data highlights the importance of using the full experimental system in the calculations, as well as including a treatment of dispersion effects in order to model correctly the observed competition between C−H activation and alkyne migratory insertion. The use of oversimplified models is particularly unrealistic in this case, while calculations on the full system that omit a dispersion correction severely overestimate the energy of the alkyne migratory insertion transition state. This is linked to the computed energy of the HOAc/alkyne substitution step, which is particularly sensitive to dispersion effects and overly endergonic in their absence. A significantly higher overall barrier to catalysis is computed for ruthenium, in which the rate-limiting process also corresponds to C−H activation. This is consistent with the harsher reaction conditions employed experimentally and reflects the need to dissociate a stronger Ru−O bond in the κ^2−κ^1-acetate displacement step that in this case leads directly to C−H bond cleavage.

The BP86-D3 calculations correctly reproduce the close competition between C−H bond activation and alkyne migratory insertion seen in the Rh system, as well as identifying C−H bond activation as being rate limiting for Ru. The calculations show that the observed deuterium isotope effects (Rh: k_H/k_D = 2.7 ± 0.5; Ru: 1.1 ± 0.2) can both be consistent with rate-limiting C−H activation due to the one- or two-step nature of the C−H activation process. For Rh the higher lying transition state corresponds to C−H bond cleavage with significant bond elongation. However, for Ru the highest lying transition state involves the κ^2−κ^1 displacement of acetate which occurs without any significant lengthening of the C−H bond. Thus, for AMLA/CMD C−H activation reactions the non-observation of a significant kinetic isotope effect does not

dx.doi.org/10.1021/jo402592z | J. Org. Chem. 2014, 79, 1954−1970

provide sufficient grounds to rule out C−H bond activation process as the rate-determining step.

EXPERIMENTAL SECTION

Unless stated otherwise, all reactions were carried out under an inert atmosphere of nitrogen, and workup was carried out in air. Electrospray (ESI) mass spectra, including high resolution, were recorded in acetonitrile or methanol. FAB mass spectra (including high resolution) were recorded with NBA as the matrix. NMR spectra were recorded on spectrometers operating at 400.13 MHz (^{1}H), [376.50 (^{19}F) and 100.61 MHz (^{13}C)] or at 500 MHz (^{1}H) [125 MHz (^{13}C)] at ambient temperature; chemical shifts (ppm) are referred to the residual protic solvent peaks and coupling constants are expressed in hertz (Hz). Assignments of ^{1}H NMR and ^{13}C NMR signals were made where possible, using appropriate standard 2-D NOESY, COSYDQF, DEPT135 or APT, HMQC(BIRD sequence) and/or HSQC experiments. All chemicals were obtained from commercial suppliers and used without further purification except [Cp*Rh(MeCN)$_3$][PF$_6$]$_2$,[34] 3-phenyl-1*H*-pyrazole,[35] 3-phenyl-5-methyl-1*H*-pyrazole and 3,5-diphenyl-1*H*-pyrazole,[36] 3-phenyl-5-(trifluoromethyl)-1*H*-pyrazole,[37] 3-(2-thiophene)-5-(trifluoromethyl)-1*H*-pyrazole,[37] and (4-nitrophenyl)but-3-yn-1-ol,[38] which were prepared using literature procedures.

General Procedure for Catalysis Reactions with Rh. [Rh(MeCN)$_3$Cp*][PF$_6$]$_2$ (33 mg, 5 mol %), the appropriate pyrazole (1 equiv), Cu(OAc)$_2$·H$_2$O (2.5 equiv), alkyne (1.2 equiv), and DCE (10 mL) were added to a Schlenk flask. The flask was sealed with a screw-cap and then transferred to a preheated oil bath and stirred at 83 °C for 16 h. The reaction mixture was cooled to room temperature with continuous stirring and diluted with Et$_2$O (10 mL).The mixture was transferred to separating funnel, and ammonium hydroxide solution (10 mL, 2 M) was added. The aqueous layer was extracted with Et$_2$O (3 × 10 mL), and the organic layers were combined and dried over MgSO$_4$. The drying agent was removed by filtration, solvent was removed under reduced pressure, and the product was purified by column chromatography.

General Procedure for Catalysis Reactions with Ru. [RuCl$_2$(*p*-cymene)]$_2$ (31 mg, 5 mol %), the appropriate pyrazole (1 equiv), AgPF$_6$ (0.2 equiv) if added, Cu(OAc)$_2$·H$_2$O (2.5 equiv), alkyne (1.2 equiv), and *t*-AmOH (3 mL) were added to a Schlenk flask. The Schlenk flask was sealed with a screw-cap and then transferred to a preheated oil bath and stirred at 120 °C for 16 h. The reaction mixture was cooled to room temperature with continuous stirring and diluted with Et$_2$O (10 mL).The mixture was transferred to separating funnel, and ammonium hydroxide solution (10 mL, 2 M) was added. The aqueous layer was extracted with Et$_2$O (3 × 10 mL), and the organic layers were combined and dried over MgSO$_4$. The drying agent was removed by filtration, solvent was removed under reduced pressure, and the product was purified by column chromatography.

Synthesis of 3aa. Following the general procedure, a Schlenk flask was loaded with [Rh(MeCN)$_3$Cp*][PF$_6$]$_2$ (22 mg, 5 mol %), 3-phenyl-5-methyl-1*H*-pyrazole (**1a**, 108 mg, 0.68 mmol), Cu(OAc)$_2$·H$_2$O (341 mg, 1.71 mmol), 4-octyne (**2a**, 90 mg, 0.43 mmol), and DCE (10 mL). The product was purified by column chromatography eluting with 70% dichloromethane in hexane to give **3aa** as a white solid (108 mg, 60%, 0.41 mmol). Mp: 62−64 °C. **3aa** was also obtained with [RuCl$_2$(*p*-cymene)]$_2$ as catalyst (173 mg, 65%, 0.65 mmol). ^{1}H NMR (400 MHz, CDCl$_3$): δ 1.08 (t, J = 7.4 Hz, 6H, CH_2CH_2Me), 1.63−1.72 (m, 2H, H^6), 1.77−1.87 (m, 2H, H^8), 2.52 (s, 3H, *Me*), 2.88−2.92 (m, 2H, H^5), 3.22−3.26 (m, 2H, H^7), 6.74 (s, 1H, *Pz-H*), 7.44 (td, J = 1.2, 7.8, 8.2 Hz, 1H, H^2), 7.50 (td, J = 1.6, 7.0, 8.2 Hz, 1H, H^3), 7.79 (brd, J = 8.6 Hz, 1H, H^4), 8.01 (dd, J = 1.2, 7.8 Hz, 1H, H^1). ^{13}C {^{1}H} NMR (100 MHz, CDCl$_3$): δ 14.2 (CH_2CH_2Me), 14.3 (CH_2CH_2Me), 14.4 (*Me*), 21.3 (C^8), 23.8 (C^6), 29.6 (C^5), 29.9 (C^7), 96.7 (Pz), 117.8, 123.5, 123.8 (C^4), 123.9 (C^1), 125.9 (C^2/C^3), 127.3 (C^2/C^3), 129.0, 136.7, 138.6, 149.4. ESIMS: m/z 267 [M + H]$^+$. HRMS (ES): calcd for $C_{18}H_{23}N_2$ [M + H]$^+$ 267.1861, found 267.1857.

Synthesis of 3aa with Catalytic Copper. A Schlenk flask was loaded with [Rh(MeCN)$_3$Cp*][PF$_6$]$_2$ (22 mg, 5 mol %), 3-phenyl-5-methyl-1*H*-pyrazole (**1a**, 108 mg, 0.68 mmol), Cu(OAc)$_2$·H$_2$O (10 mg, 10 mol %, 0.05 mmol), 4-octyne (**2a**, 90 mg, 0.43 mmol), and DCE (10 mL). The crude ^{1}H NMR spectrum showed the presence of two products in a 3:1 ratio. The products were purified by column chromatography eluting from 100% dichloromethane to 10% ethyl acetate in dichloromethane to give **3aa** (133 mg, 50%, 0.50 mmol) and **4aa** as a yellow oil (65 mg, 24%, 0.24 mmol).

4aa. ^{1}H NMR (400 MHz, CDCl$_3$): δ 0.82 (t, J = 7.4 Hz, 3H, CH_2CH_2Me), 1.10 (t, J = 7.4 Hz, 3H, CH_2Me), 1.23−1.31 (m, 2H, CH_2CH_2Me), 1.51−1.61 (m, 1H, CH_2CH_2Me), 1.67−1.76 (m, 1H, CH_2CH_2Me), 2.23 (sext, J = 7.4 Hz, 1H, CH_2Me), 2.32 (s, 3H, *Me*), 2.38 (sext, J = 7.4 Hz, 1H, CH_2Me), 5.34 (dd, J = 5.9, 7.8 Hz, 1H, N−*CH*), 6.02 (t, J = 7.4 Hz, 1H, C=*CH*), 6.29 (s, 1H, *Pz-H*), 7.23−7.30 (m, 2H, H^2, H^3), 7.46−7.49 (m, 1H, H^1), 7.51−7.54 (m, 1H, H^4). ^{13}C {^{1}H} NMR (125 MHz, CDCl$_3$): δ 13.7 (CH_2CH_2Me), 14.0 (CH_2Me), 14.0 (*Me*), 18.7 (CH_2CH_2Me), 21.2 (CH_2Me), 38.8 (CH_2CH_2Me), 57.9 (N-*CH*), 99.7 (Pz), 123.5 (C^1), 125.0 (C^4), 125.2, 127.8 (C^2/C^3), 128.2 (C^2/C^3), 131.9, 132.6, 132.7 (C=*CH*), 138.0, 148.3. ESIMS: m/z 267 [M + H]$^+$. HRMS (ES): calcd for $C_{18}H_{23}N_2$ [M + H]$^+$ 267.1861, found 267.1849

Synthesis of 3ba. Following the general procedure, a Schlenk flask was loaded with [Rh(MeCN)$_3$Cp*][PF$_6$]$_2$ (33 mg, 5 mol %), 3-phenyl-1*H*-pyrazole (**1b**, 144 mg, 1 mmol), Cu(OAc)$_2$·H$_2$O (500 mg, 2.5 mmol), 4-octyne (**2a**, 132 mg, 1.2 mmol), and DCE (10 mL). The product was purified by column chromatography eluting with 50% ethyl acetate in hexane to give **3ba** as a white solid (219 mg, 87%, 0.87 mmol). ^{1}H NMR (400 MHz, CDCl$_3$): δ 1.11 (t, J = 7.0, 7.4 Hz, 6H, H^9, H^{12}), 1.70 (sext, J = 7.0, 7.8 Hz, 2H, H^8), 1.83 (sext, J = 7.4, 8.2 Hz, 2H, H^{11}), 2.93−2.97 (m, 2H, H^7), 3.26−3.30 (m, 2H, H^{10}), 6.99 (d, J = 2.3 Hz, 1H, H^2), 7.50 (td, J = 1.6, 7.8 Hz, 1H, H^4), 7.55 (td, J = 1.2, 8.2 Hz, 1H, H^5), 7.84 (br dd, J = 0.8, 8.2 Hz, 1H, H^6), 7.95 (d, J = 2.3 Hz, 1H, H^1), 8.11 (dd, J = 1.6, 7.8 Hz, 1H, H^3), ^{13}C {^{1}H} NMR (100 MHz, CDCl$_3$): δ 14.4 (C^9), 14.5 (C^{12}), 21.3 (C^{11}), 23.8 (C^8), 29.7 (C^7), 30.1 (C^{10}), 97.1 (C^2), 119.1, 123.9, 124.0 (C^3,C^6), 126.3 (C^5), 127.6 (C^4), 129.0, 136.8, 137.8, 139.9 (C^1). ESIMS: m/z 253 [M + H]$^+$. HRMS (ES): calcd for $C_{17}H_{21}N_2$ [M + H]$^+$ 253.1705, found 253.1705.

Synthesis of 3ca. Following the general procedure, a Schlenk flask was loaded with [Rh(MeCN)$_3$Cp*][PF$_6$]$_2$ (33 mg, 5 mol %), 3,5-diphenyl-1*H*-pyrazole (**1c**, 220 mg, 1 mmol), Cu(OAc)$_2$·H$_2$O (500 mg, 2.5 mmol), 4-octyne (**2a**, 132 mg, 1.2 mmol), and DCE (10 mL). The product was purified by column chromatography eluting from 40% dichloromethane in petroleum spirit (40−60 °C) to give **3ca** as a white solid (298 mg, 91%, 0.91 mmol). Mp: 85−87 °C. ^{1}H NMR (300 MHz, CDCl$_3$): δ 1.11 (t, J = 5.6, 7.3 Hz, 3H, H^{10}), 1.14 (t, J = 5.6, 7.3 Hz, 3H, H^{13}), 1.65−1.78 (m, 2H, H^9), 1.83−1.96 (m, 2H, H^{12}), 2.93−2.98 (m, 2H, H^8), 3.31−3.36 (m, 2H, H^{11}), 7.28 (s, 2H, *Pz-H*), 7.35 (tt, J = 1.2, 7.4, 8.6 Hz, 1H, H^1), 7.46 (tt, J = 1.2, 7.4 Hz, 2H, H^2), 7.50 (td, J = 1.6, 7.4, 8.6 Hz, 1H, H^6), 7.55 (br td, J = 1.6, 7.0, 8.6 Hz, 1H, H^5), 7.84 (dd, J = 1.6, 7.4 Hz, 1H, H^7), 8.06 (dd, J = 1.2, 8.2 Hz, 2H, H^3), 8.13 (dd, J = 2.0, 7.0 Hz, 1H, H^4). ^{13}C {^{1}H} NMR (100 MHz, CDCl$_3$): δ 14.5 (C^{10}, C^{13}), 21.3 (C^{12}), 23.8 (C^9), 29.8 (C^8), 30.0 (C^{11}), 94.1 (Pz), 119.0, 123.8, 123.9 (C^4), 124.0 (C^7), 126.2, 126.3 (C^3), 127.6 (C^5), 127.9 (C^6), 128.7 (C^2), 129.1 (C^1), 133.9, 137.0, 139.0, 151.3. ESIMS: m/z 329 [M + H]$^+$. FAB MS: m/z 329 [M + H]$^+$, 299 [M-2(Me)]$^+$, 271 [M-2(Me)-2(CH$_2$)]$^+$. HRMS (ES): calcd for $C_{23}H_{25}N_2$ [M + H]$^+$ 329.2018, found 329.2012.

Synthesis of 3da. Following the general procedure, a Schlenk flask was loaded with [Rh(MeCN)$_3$Cp*][PF$_6$]$_2$ (33 mg, 5 mol %), 3-phenyl-5-(trifluoromethyl)-1*H*-pyrazole (**1d**, 212 mg, 1.0 mmol), Cu(OAc)$_2$·H$_2$O (500 mg, 2.5 mmol), 4-octyne (**2a**, 110 mg, 1.2 mmol), and DCE (10 mL). The crude ^{1}H NMR spectrum showed the presence of two products in a 17:1 ratio. The products were purified by column chromatography eluting from 50% dichloromethane in petroleum ether (40−60 °C) to 100% dichloromethane to give **3da** as a white powder (255 mg, 80%, 0.80 mmol). Mp: 63−65 °C. ^{1}H NMR (400 MHz, CDCl$_3$): δ 1.09 (t, J = 7.4 Hz, 3H, H^{10}), 1.11 (t, J = 7.0, 7.4 Hz, 3H, H^7), 1.65−1.75 (m, 2H, H^6), 1.77−1.86 (m, 2H, H^9), 2.93−2.98 (m, 2H, H^5), 3.25−3.29 (m, 2H, H^8), 7.21 (s, 1H, *Pz-H*), 7.54 (td, J = 7.0, 7.4 Hz, 1H, H^2), 7.60 (td, J = 7.0, 7.4 Hz, 1H, H^3), 7.87

dx.doi.org/10.1021/jo402592z | J. Org. Chem. 2014, 79, 1954−1970

(br d, J = 2.0 Hz, 1H, H^4), 8.08 (dt, J = 2.0 Hz, 1H, H^1). ^{13}C {^1H} NMR (100 MHz, $CDCl_3$): δ 14.2 (C^7/C^{10}), 14.4 (C^7/C^{10}), 21.2 (C^9), 23.7 (C^6), 29.8 (C^5, C^8), 95.6 (Pz), 121.4, 121.9 (q, J = 273.6 Hz,CF_3), 123.5, 123.2, 123.9 (C^1), 124.2 (C^4), 126.9 (C^2), 128.4 (C^3), 129.1, 136.8, 138.5, 142.4 (q, J = 39.2 Hz,C-CF_3). ^{19}F {^1H} NMR (376 MHz, $CDCl_3$): δ −61.4 (CF_3). HRMS (ES): calcd for $C_{18}H_{20}N_2F_3$ [M + H]$^+$321.1579, found 321.1566.The product was recrystallized from dichloromethane/hexane to give **3da** as clear needles.

Synthesis of 3ab. Following the general procedure, a Schlenk flask was loaded with [Rh(MeCN)$_3$Cp*][PF$_6$]$_2$ (10 mg, 5 mol %), 3-phenyl-5-methyl-1H-pyrazole (**1a**, 50 mg, 0.32 mmol), Cu(OAc)$_2$·H$_2$O (161 mg, 0.81 mmol), diphenylacetylene (**2b**, 68 mg, 0.38 mmol), and DCE (10 mL). The product was purified by column chromatography eluting from 70% dichloromethane in hexane to give **3ab** as an orange solid (97 mg, 91%, 0.29 mmol). Compound **3ab** was also obtained with [RuCl$_2$(p-cymene)]$_2$ as catalyst with AgPF$_6$ (25 mg, 0.1 mmol) as additive (yield 14%, based on NMR integration against an internal standard). ^1H NMR (400 MHz, $CDCl_3$): δ 3.71 (s, 3H, *Me*), 6.89 (s, 1H, *Pz-H*), 7.15−7.18 (dd, J = 1.2, 7.4 Hz, 2H, *Ar-H*), 7.21−7.27 (m, 4H, *Ar*−*H*), 7.31−7.33 (m, 3H, *Ar-H*), 7.37−7.39 (m, 2H, *Ar-H*), 7.50−7.54 (m, 2H, H^2, *Ar-H*), 8.11 (d, J = 7.4 Hz, 1H, H^1). ^{13}C {^1H} NMR (100 MHz, $CDCl_3$): δ 43.4 (*Me*), 97.4 (Pz), 122.9 (Ar), 123.3 (Ar), 123.5 (Ar), 126.6 (Ar), 127.0 (Ar), 127.1 (Ar), 127.5 (Ar), 127.7 (Ar), 127.9 (Ar), 128.2 (Ar), 128.2 (Ar), 128.3 (Ar), 128.7, 130.0 (Ar), 131.1 (Ar), 131.6 (Ar), 131.7 (Ar), 133.2 (Ar), 136.2 (Ar), 136.5, 139.4, 150.7. ESIMS: m/z 335 [M + H]$^+$. HRMS (ES): calcd for $C_{24}H_{19}N_2$ [M + H]$^+$ 335.1548, found 335.1541.

Synthesis of 3bb. Following the general procedure, a Schlenk flask was loaded with [Rh(MeCN)$_3$Cp*][PF$_6$]$_2$ (33 mg, 5 mol %), 3-phenyl-1H-pyrazole (**1b**, 144 mg, 1 mmol), Cu(OAc)$_2$·H$_2$O (500 mg, 2.5 mmol), diphenylacetylene (**2b**, 214 mg, 1.2 mmol), and DCE (10 mL). The product was purified by column chromatography with ethyl acetate/dichloromethane as eluant to give **3bb** as a white solid (250 mg, 78%, 0.78 mmol). ^1H NMR (400 MHz, $CDCl_3$): δ 7.13 (d, J = 2.0 Hz, 1H, H^2), 7.19−7.22 (m, 2H, *Ar-H*), 7.26−7.35 (m, 8H, *Ar-H*), 7.40−7.43 (m, 1H, *Ar-H*), 7.44 (td, J = 1.2, 6.7, 7.0 Hz, 1H, H^5), 7.58 (td, J = 2.0, 6.7, 8.2 Hz, 1H, H^4), 7.98 (d, J = 2.0 Hz, 1H, H^1), 8.21 (m, 1H, H^3), ^{13}C {^1H} NMR (100 MHz, $CDCl_3$): δ 97.6 (C^2), 123.6 (C^3), 124.1, 126.7 (C^5), 127.2 (C^4), 127.4, 127.7, 127.9, 128.01, 128.4, 130.9, 131.6, 141.1 (C^1). ESIMS: m/z 321 [M + H]$^+$. HRMS (ES): calcd for $C_{23}H_{17}N_2$ [M + H]$^+$321.1392, found 321.1394.

Synthesis of 3cb. Following the general procedure, a Schlenk flask was loaded with [RhCp*(MeCN)$_3$][PF$_6$]$_2$ (33 mg, 5 mol %), 3,5-diphenyl-1H-pyrazole (**1c**, 220 mg, 1.0 mmol), Cu(OAc)$_2$·H$_2$O (500 mg, 2.5 mmol), diphenylacetylene (**2b**, 214 mg, 1.2 mmol), and DCE (10 mL). The product was purified by column chromatography eluting from 100% dichloromethane to give **3cb** as an orange solid (390 mg, 98%, 0.98 mmol). ^1H NMR (400 MHz, $CDCl_3$): δ 7.21 (dd, J = 1.6, 7.4 Hz, 2H, *Ar*−*H*), 7.26−7.34 (m, 6H), 7.36−7.44 (m, 6H, *Ar-H*), 7.42 (s, 1H, *Pz-H*), 7.56−7.60 (m, 1H, *Ar-H*), 7.92 (dd, J = 1.2, 7.0 Hz, 2H, *Ar-H*), 8.23 (d, J = 7.8 Hz, 1H, *Ar-H*), ^{13}C {^1H} NMR (100 MHz, $CDCl_3$): δ 94.6 (Pz), 123.6, 124.0, 126.8, 127.1, 127.3, 127.5, 127.7, 128.0, 128.1, 128.4, 128.6, 130.0, 131.4, 131.8, 133.0,133.5, 136.4,139.9, 152.3. ESIMS: m/z 397[M + H]$^+$. HRMS (ES): calcd for $C_{29}H_{21}N_2$ [M + H]$^+$397.1705, found 397.1711.The product was recrystallized from standing in chloroform to give **3cb** as orange blocks. Anal. Calcd for ($C_{29}H_{21}N_2$): C, 87.85; H, 5.08; N, 7.07. Found: C, 87.99; H, 4.95; N, 6.95%.

Synthesis of 3db. Following the general procedure, a Schlenk flask was loaded with [Rh(MeCN)$_3$Cp*][PF$_6$]$_2$ (16 mg, 5 mol %), 3-phenyl-5-(trifluoromethyl)-1H-pyrazole (**1d**, 106 mg, 0.50 mmol), Cu(OAc)$_2$·H$_2$O (250 mg, 1.25 mmol), diphenylacetylene (**2b**, 107 mg, 0.60 mmol), and DCE (5 mL). The product was purified by column chromatography eluting from 50% dichloromethane in petroleum ether (40−60 °C) to give **3db** as a white powder (175 mg, 90%, 0.45 mmol). ^1H NMR (400 MHz, $CDCl_3$): δ 7.18 (dd, J = 2.3, 7.8 Hz, 2H, H^5), 7.24−7.33 (m, 8H, *Ar-H*), 7.36 (s, 1H, *Pz-H*), 7.45 (dd, J = 1.6, 8.2 Hz, 1H, H^4), 7.49 (td, J = 1.2, 7.0, 8.2 Hz, 1H, H^3), 7.62 (td, J = 1.2, 7.0, 8.2 Hz, 1H, H^2), 8.20 (dd, J = 1.2, 8.2 Hz, 1H, H^1). ^{13}C {^1H} NMR (125 MHz, $CDCl_3$): δ 95.9 (Pz), 121.6 (q, J = 270.1 Hz, CF_3), 123.4 (C^1), 123.6, 126.0, 126.9 (C^4), 127.3 (Ar), 127.6 (Ar), 127.8 (C^2), 128.0 (Ar), 128.3 (C^3), 128.4 (Ar), 129.9, 131.0 (Ar), 131.2 (C^5), 131.8, 135.5, 136.2, 139.2, 143.3 (q, J = 38.0 Hz, CF_3). ^{19}F {^1H} NMR (376 MHz, $CDCl_3$): δ −61.3 (CF_3). ESIMS: m/z 389 [M + H]$^+$. HRMS (ES): calcd for $C_{24}H_{16}N_2F_3$ [M + H]$^+$389.1266, found 389.1263. The product was recrystallized from dichloromethane/hexane to give **3db** as clear crystals.

Synthesis of 3ac and 3ac′. Following the general procedure, a Schlenk flask was loaded with [Rh(MeCN)$_3$Cp*][PF$_6$]$_2$ (33 mg, 5 mol %), 3-phenyl-5-methyl-1H-pyrazole (**1a**, 158 mg, 1.00 mmol), Cu(OAc)$_2$·H$_2$O (500 mg, 2.50 mmol), 1-phenyl-1-propyne (**2c**, 139 mg, 1.20 mmol), and DCE (10 mL). The crude ^1H NMR spectrum showed the presence of three products in a 12:9:1 ratio. The products were purified by column chromatography eluting with 30% ethyl acetate in hexane to give **3ac** as an orange powder (122 mg, 45%, 0.45 mmol) (mp 98−101 °C), **3ac′** as orange oil (impure), and isomer **6ac** as an orange powder (110 mg, 40%, 0.40 mmol). Compound **3ac′** was purified further by preparative TLC eluting with 30% ethyl acetate in hexane to give **3ac′** as an orange oil (13 mg, 5%, 0.05 mmol). Compounds **3ac** and **3ac′** (218 mg, 80%, 0.80 mmol) were obtained with [RuCl$_2$(p-cymene)]$_2$ as catalyst in a 12:1 ratio and purified by column chromatography to give **3ac** (182 mg, 67%, 0.67 mmol).

3ac. ^1H NMR (400 MHz, $CDCl_3$): δ 2.29 (s, 3H, C═C*Me*), 2.41 (s, 3H, *Me*), 6.79 (s, 1H, *Pz-H*), 7.45−7.50 (m, 5H, H^5, H^6, H^7), 7.51−7.56 (m, 2H, H^2, H^3), 7.84−7.86 (m, 1H, H^4), 8.06−8.09 (m, 1H, H^1). ^{13}C {^1H} NMR (100 MHz, $CDCl_3$): δ 14.3 (*Me*), 15.0 (C═C*Me*), 97.0 (Pz), 115.0, 123.8 (C^1), 123.9, 124.3 (C^4), 127.0 (C^2/C^3), 127.6 (C^2/C^3), 128.5 (C^5/C^6), 128.7 (C^7), 129.9, 130.6 (C^5/C^6), 134.0, 135.8, 138.9, 150.0. ESIMS: m/z 273 [M + H]$^+$. HRMS (ES): calcd for $C_{19}H_{17}N_2$ [M + H]$^+$ 273.1392, found 273.1392.

3ac′. ^1H NMR (400 MHz, $CDCl_3$): δ 2.56 (s, 3H, C═C*Me*), 2.59 (s, 3H, *Me*), 6.88 (s, 1H, *Pz-H*), 7.24 (br d, J = 7.8 Hz, 1H, H^4), 7.34 (dt, J = 2.0, 6.7, 8.6 Hz, 2H, H^5), 7.35−7.39 (m, 1H, H^3), 7.44−7.53 (m, 4H, H^2, H^6, H^7), 8.08 (dd, J = 0.8, 7.8 Hz, 1H, H^1). ^{13}C {^1H} NMR (100 MHz, $CDCl_3$): δ 14.2 (*Me*), 15.9 (C═C*Me*), 97.4 (Pz), 121.6, 122.8, 123.4 (C^1), 126.0 (C^4), 126.2 (Ar), 127.4 (C^3), 127.6 (Ar), 128.6 (C^6), 129.9, 131.0 (C^5), 133.1, 137.1, 139.0, 150.3. ESIMS: m/z 273 [M + H]$^+$. HRMS (ES): calcd for $C_{19}H_{17}N_2$ [M + H]$^+$ 273.1392, found 273.1409.

6ac. ^1H NMR (400 MHz, $CDCl_3$): δ 2.32 (s, 3H,*Me*), 5.49 (s, 1H, C═CH_2), 5.67 (s, 1H, C═CH_2), 6.15 (s, 1H, C*H*(Ph)), 6.42 (s, 1H, *Pz-H*), 6.94 (dd, J = 2.3, 8.2 Hz, 2H, H^5), 7.14−7.20 (m, 3H, H^6, H^7), 7.22 (td, J = 1.2, 7.4, 7.8 Hz, 1H, H^3), 7.32 (td, J = 1.2, 7.4, 7.8 Hz, 1H, H^2), 7.52 (dd, J = 1.2, 7.8 Hz, 1H, H^4), 7.54 (dd, J = 1.2, 7.8 Hz, 1H, H^1). ^{13}C {^1H} NMR (100 MHz, $CDCl_3$): δ 13.8 (*Me*), 66.4 (*C*H(Ph)), 100.5 (Pz), 115.3 (C═*C*H$_2$), 123.7 (C^4), 125.5 (C^5), 125.5, 127.6 (C^7), 128.4 (C^3), 128.5 (C^2), 128.6 (C^6), 128.8 (C^1), 129.1, 129.8, 139.0, 140.6, 142.3, 149.6. ESIMS: m/z 273 [M + H]$^+$. HRMS (ES): calcd for $C_{19}H_{17}N_2$ [M + H]$^+$ 273.1392, found 273.1391.

Synthesis of 3bc and 3bc′. Following the general procedure, a Schlenk flask was loaded with [Rh(MeCN)$_3$Cp*][PF$_6$]$_2$ (33 mg, 5 mol %), 3-phenyl-1H-pyrazole (**1b**, 144 mg, 1 mmol), Cu(OAc)$_2$·H$_2$O (500 mg, 2.5 mmol), 1-phenyl-1-propyne (**2c**, 139 mg, 1.2 mmol), and DCE (10 mL). The crude ^1H NMR spectrum showed the presence of free pyrazole and two products in a 12:1 ratio. The products were purified by column chromatography eluting from 100% dichloromethane to 20% ethyl acetate in petroleum ether (40−60 °C) to give **3bc′** as orange oil (impure) and **3bc** as an orange powder (111 mg, 79% (based on 54% conversion), 0.43 mmol).

3bc′. This was obtained in a mixture with **3bc**. ^1H NMR (400 MHz, $CDCl_3$): δ 2.59 (s, 3H, *Me*), 7.09 (d,J = 2.3 Hz, 1H, H^2), 7.24−7.27 (m, 1H, *Ar-H*), 7.33 (dd, J = 1.6, 8.2 Hz, 1H, H^3/H^6), 7.39 (td, J = 1.6, 7.0, 8.2 Hz, 1H, H^4/H^5), 7.45−7.62 (m, 6H, *Ar-H*), 8.04 (d, J = 2.0 Hz, 1H, H^1).

3bc. ^1H NMR (400 MHz, $CDCl_3$): δ 2.35 (s, 3H, *Me*), 7.03 (d, J = 2.3 Hz, 1H, H^2), 7.46−7.57 (m, 5H, *Ar*−*H*), 7.58−7.61 (m, 2H, H^4, H^5), 7.88 (d, J = 2.0 Hz, 1H, H^1), 7.89−7.92 (m, 1H, H^6), 8.15−8.17 (m, 1H, H^3). ^{13}C {^1H} NMR (100 MHz, $CDCl_3$): δ 14.8 (*Me*), 97.1 (C^2), 116.1, 123.7 (C^3), 124.0, 124.3 (C^6), 127.0 (C^4/C^5), 127.7 (C^4/C^5), 128.5, 128.7 (Ar), 129.7 (Ar), 130.2 (Ar), 133.7, 135.8, 137.8,

dx.doi.org/10.1021/jo402592z | J. Org. Chem. 2014, 79, 1954−1970

140.3 (C^1). HRMS (ES): calcd for $C_{18}H_{14}N_2$ $[M + H]^+$ 259.1341, found 259.1336.

Synthesis of 3cc and 3cc′. Following the general procedure, a Schlenk flask was loaded with $[Rh(MeCN)_3Cp^*][PF_6]_2$ (33 mg, 5 mol %), 3,5-diphenyl-1*H*-pyrazole (**1c**, 220 mg, 1 mmol), $Cu(OAc)_2{\cdot}H_2O$ (500 mg, 2.50 mmol), 1-phenyl-1-propyne (**2c**, 139 mg, 1.20 mmol), and DCE (10 mL). The crude ^{1}H NMR spectrum showed the presence of two products in a 3:1 ratio. The products were purified by column chromatography eluting from 50% dichloromethane in petroleum ether (40−60 °C) to 100% dichloromethane to give **3cc** and **3cc′** (219 mg, 66% combined yield, 0.66 mmol). Compound **3cc′** was obtained pure as a brown solid (35 mg, 10%, 0.10 mmol) and **3cc** as an orange solid (147 mg, 44%, 0.44 mmol). Mp: 145−148 °C.

3cc′. ^{1}H NMR (400 MHz, $CDCl_3$): δ 2.64 (s, 3H, *Me*), 7.26 (d, J = 8.2 Hz, 1H, H^7), 7.34−7.42 (m, 4H, H^1, H^6, H^8), 7.39 (s, 1H, *Pz-H*), 7.46−7.55 (m, 6H, H^2, H^5, H^9, H^{10}), 8.07 (dd, J = 1.6, 8.6 Hz, 2H, H^3), 8.18 (br dt, J = 1.2, 2.0, 7.8 Hz, 1H, H^4). ^{13}C {^{1}H} NMR (100 MHz, $CDCl_3$): δ 15.8 (*Me*), 94.8 (Pz), 122.5, 123.2, 123.5 (C^4), 126.2 (C^7), 126.4 (C^3), 127.6 (Ar), 127.7 (Ar), 128.2 (Ar), 128.7 (C^2/C^9), 128.7 (C^2/C^9), 130.0, 131.0 (C^8), 133.6, 133.7, 137.1, 139.5, 152.2. ESIMS: m/z 334 $[M + H]^+$. HRMS (ES): calcd for $C_{24}H_{19}N_2$ $[M + H]^+$ 335.1548, found 335.1557.

3cc. ^{1}H NMR (400 MHz, $CDCl_3$): δ 2.37 (s, 3H, *Me*), 7.27 (tt, J = 1.2, 2.7, 6.7, 8.2 Hz, 1H, H^1), 7.32 (s, 1H, *Pz-H*), 7.35−7.37 (m, 2H, H^2), 7.50−7.55 (m, 5H, H^8, H^9, H^{10}), 7.57−7.60 (m, 1H, H^5/H^6), 7.60−7.62 (m, 1H, H^5/H^6), 7.87 (dd, J = 1.2, 8.2 Hz, 2H, H^3), 7.89−7.91 (m, 1H, H^7), 8.16−8.20 (m, 1H, H^4). ^{13}C {^{1}H} NMR (125 MHz, $CDCl_3$): δ 15.2 (*Me*), 94.3 (Pz), 116.1, 123.7 (C^4), 123.8, 124.1 (C^7), 124.5 (C^3), 127.2 ($C^1/C^5/C^6$), 127.8 ($C^1/C^5/C^6$), 127.9 ($C^1/C^5/C^6$), 128.2 (C^2/C^9), 128.5 (C^2/C^9), 128.6 (C^{10}), 130.0, 130.9 (C^8), 133.6, 133.7, 136.1, 139.3, 151.6. ESIMS: m/z 334 $[M + H]^+$. HRMS (ES): calcd for $C_{24}H_{19}N_2$ $[M + H]^+$335.1548, found 335.1560. The product was recrystallized from dichloromethane/hexane to give **3cc** as orange blocks.

Synthesis of 3dc and 3dc′. Following the general procedure, a Schlenk flask was loaded with $[Rh(MeCN)_3Cp^*][PF_6]_2$ (33 mg, 5 mol %), 3-phenyl-5-(trifluoromethyl)-1*H*-pyrazole (**1d**, 212 mg, 1.0 mmol), $Cu(OAc)_2{\cdot}H_2O$ (500 mg, 2.5 mmol), 1-phenyl-1-propyne (**2c**, 139 mg, 1.2 mmol), and DCE (10 mL). The crude ^{1}H NMR spectrum showed the presence of three products in a 7:2:1 ratio. The products were purified by column chromatography eluting from 50% dichloromethane in petroleum ether (40−60 °C) to give **3dc′** as an orange solid (30 mg, 9%, 0.09 mmol), **3dc** as an orange powder (178 mg, 55%, 0.55 mmol) (mp 135−137 °C), and isomer **6dc** as an orange oil (53 mg, 16%, 0.16 mmol) which was purified further by preparative TLC eluting with 50% dichloromethane in petroleum ether (40−60 °C).

3dc′. ^{1}H NMR (400 MHz, $CDCl_3$): δ 2.60 (s, 3H, *Me*), 7.28−7.34 (m, 4H, *Pz-H*, H^4,H^5), 7.44−7.58 (m, 5H, H^2,H^3, H^6,H^7), 8.16 (d, J = 7.4 Hz, 1H, H^1). ^{13}C {^{1}H} NMR (100 MHz, $CDCl_3$): δ 15.7 (*Me*), 96.2 (Pz), 119.3 (q, J = 299.8 Hz, CF_3), 123.0, 123.5 (C^1), 124.8, 126.5 (Ar), 127.2 (Ar), 128.1 (Ar), 128.4 (Ar), 128.8 (Ar), 130.0, 130.7 (Ar), 133.5, 136.3, 138.9, 143.1 (q, J = 35.9 Hz, *C*-CF_3), ^{19}F {^{1}H} NMR (376 MHz, $CDCl_3$): δ −61.4 (CF_3). HRMS (ES): calcd for $C_{19}H_{14}N_2F_3$ $[M + H]^+$ 327.1109, found 327.1109.

3dc. ^{1}H NMR (400 MHz, $CDCl_3$): δ 2.37 (s, 3H, *Me*), 7.25 (s, 1H, *Pz-H*), 7.45 (dd, J = 2.0, 7.8 Hz, 2H, H^5), 7.49−7.55 (m, 3H, H^6,H^7), 7.60−7.67 (m, 2H, H^2,H^3), 7.91−7.94 (m, 1H, H^4), 8.12−8.14 (m, 2H, H^1). ^{13}C {^{1}H} NMR (100 MHz, $CDCl_3$): δ 15.3 (*Me*), 95.9 (Pz), 118.7, 121.7 (q, J = 268.9 Hz, CF_3), 123.8, 123.8 (C^1), 124.7 (C^4), 127.8 (C^2/C^3), 128.5 (C^6), 128.7 (C^2/C^3), 129.0 (C^7), 129.9, 130.8 (C^5), 132.7, 135.9, 138.8, 143.1 (q, J = 39.5 Hz, *C*-CF_3). ^{19}F {^{1}H} NMR (376 MHz, $CDCl_3$): δ −61.2 (CF_3). HRMS (ES): calcd for $C_{19}H_{14}N_2F_3$ $[M + H]^+$ 327.1109, found 327.1114. The product was recrystallized from dichloromethane/hexane to give **3dc** as orange blocks.

6dc. ^{1}H NMR (400 MHz, $CDCl_3$): δ 5.56 (d, J = 0.8 Hz, 1H, H^6), 5.76 (s, 1H, H^5), 6.27 (s, 1H, N−*CH*), 6.87 (s, 3H, *Pz-H*), 6.94−6.96 (m, 2H, H^7), 7.17−7.21 (m, 3H, H^8,H^9), 7.32 (td, J = 1.6, 7.4 Hz, 1H, H^2/H^3), 7.38 (td, J = 1.6, 7.4, 7.8 Hz, 1H, H^2/H^3), 7.56−7.60 (m, 2H, H^1, H^4). ^{13}C {^{1}H} NMR (100 MHz, $CDCl_3$): δ 67.0 (N-CH), 99.4 (Pz), 116.8 (C=CH_2), 121.4 (q, J = 268.7 Hz,CF_3), 124.0 (C^1/C^4), 124.3, 125.5 (C^7), 125.7 (C^1/C^4), 128.0 (C^8/C^9), 128.5 (C^8/C^9), 129.0 (C^2/C^3), 129.5 (C^2/C^3), 129.6, 139.1, 139.7, 141.1, 142.8 (q, J = 40.9 Hz, *C*-CF_3). ^{19}F {^{1}H} NMR (376 MHz, $CDCl_3$): δ −61.9 (CF_3). HRMS (ES): calcd for $C_{19}H_{14}N_2F_3$ $[M + H]^+$ 327.1109, found 327.1123.

Synthesis of 3ad and 3ad′. Following the general procedure, a Schlenk flask was loaded with $[Rh(MeCN)_3Cp^*][PF_6]_2$ (26 mg, 5 mol %), 3-phenyl-5-methyl-1*H*-pyrazole (**1a**, 125 mg, 0.79 mmol), $Cu(OAc)_2{\cdot}H_2O$ (395 mg, 1.98 mmol), (4-nitrophenyl)but-3-yn-1-ol (**2d**, 182 mg, 0.95 mmol), and DCE (10 mL). The crude ^{1}H NMR spectrum showed the presence of two products in a 3:1 ratio. Column chromatography eluting from 1% ethyl acetate in dichloromethane gave a mixture of regioisomers (264 mg, 96%, 0.76 mmol). Recrystallization from dichloromethane/hexane gave **3ad** as yellow crystals (200 mg, 73%, 0.73 mmol). Mp: 170−172 °C.

3ad. ^{1}H NMR (400 MHz, $CDCl_3$): δ 1.36 (br s, 1H, O*H*), 2.39 (s, 3H, *Me*), 3.00 (t, J = 7.0 Hz, 2H, CH_2CH_2OH), 3.83 (br t, J = 5.9 Hz, 2H, CH_2CH_2OH), 6.83 (s, 1H, *Pz-H*), 7.60 (t, J = 3.1 Hz, 1H, H^2/H^3), 7.62 (t, J = 3.5 Hz, 2H, H^2/H^3), 7.69 (d, J = 9.0 Hz, 2H, H^5), 7.93 (dd, J = 3.1 Hz, 1H, H^4), 8.11 (dd, J = 3.1 Hz, 1H, H^1), 8.42 (d, J = 9.0 Hz, 2H, H^6). ^{13}C {^{1}H} NMR (100 MHz, $CDCl_3$): δ 14.2 (*Me*), 31.3 (CH_2CH_2OH), 62.3 (CH_2CH_2OH), 97.5 (Pz), 115.9, 124.0 (C^6), 124.3 (C^1), 124.3 (C^4), 124.4, 127.7 (C^2/C^3), 128.0 (C^2/C^3), 128.4, 131.8 (C^5), 135.0, 139.1, 140.4, 148.1, 150.8. ESIMS: m/z 348 $[M + H]^+$. HRMS (ES): calcd for $C_{20}H_{18}N_3O_3$ $[M + H]^+$ 348.1348, found 348.1348. The product was recrystallized from dichloromethane/hexane to give **3ad** as orange needles. Anal. Calcd for ($C_{20}H_{17}N_3O_3$): C, 69.15; H, 4.93; N, 12.10. Found: C, 68.99; H, 4.80; N, 11.98.

3ad′. Recrystallization with dichloromethane/hexane left a filtrate of **3ad′** in a mixture with **3ad**. ^{1}H NMR (400 MHz, $CDCl_3$): δ 1.36 (br s, 1H, O*H*), 2.39 (s, 3H, *Me*), 3.00 (t, J = 7.0 Hz, 2H, CH_2CH_2OH), 3.83 (br t, J = 5.9 Hz, 2H, CH_2CH_2OH), 6.83 (s, 1H, *Pz-H*), 7.04 (d, J = 8.2 Hz, 1H, H^1/H^4), 7.93−7.43 (m, 1H, H^2/H^3), 7.53−7.56 (m, 1H, H^2/H^3), 7.54 (d, J = 9.0 Hz, 2H, H^5), 8.11 (d, J = 7.4 Hz, 1H, H^1/H^4), 8.41 (d, J = 9.0 Hz, 2H, H^6).

Synthesis of 3cd and 3cd′. Following the general procedure, a Schlenk flask was loaded with $[Rh(MeCN)_3Cp^*][PF_6]_2$ (16 mg, 5 mol %), 3,5-diphenyl-1*H*-pyrazole (**1c**, 110 mg, 0.5 mmol), $Cu(OAc)_2{\cdot}H_2O$ (250 mg, 1.25 mmol), (4-nitrophenyl)but-3-yn-1-ol (**2d**, 115 mg, 0.6 mmol), and DCE (5 mL). The crude ^{1}H NMR spectrum showed the presence of two products in a 3:1 ratio. The products were purified by column chromatography eluting with 50% ethyl acetate in hexane to give **3cd** as a yellow solid (90 mg, 44%, 0.22 mmol) (mp 200−202 °C), and **3cd′** as a yellow solid (80 mg, 39%, 0.20 mmol). Mp: 175−178 °C.

3cd. ^{1}H NMR (400 MHz, $CDCl_3$): δ 1.54 (br s,1H, O*H*), 3.08 (t, J = 7.0 Hz, 2H, CH_2CH_2OH), 3.87 (br q, J = 6.7 Hz, 2H, CH_2CH_2OH), 7.30 (tt, J = 1.2, 7.4, 8.6 Hz, 1H, H^7), 7.35 (s, 1H, *Pz-H*), 7.37 (tt, J = 1.2, 1.6, 7.0, 7.4 Hz, 2H, H^6), 7.62−7.68 (m, 2H, H^2, H^3), 7.76 (d, J = 8.6 Hz, 2H, H^8), 7.83 (dd, J = 1.6, 7.0 Hz, 2H, H^5), 7.97−8.00 (m, 1H, H^4), 8.21−8.24 (m, 1H, H^1), 8.42 (d, J = 8.6 Hz, 2H, H^9). ^{13}C {^{1}H} NMR (100 MHz, $CDCl_3$): δ 31.2 (CH_2CH_2OH), 62.0 (CH_2CH_2OH), 94.5 (Pz), 116.8, 123.5 (C^9), 124.1 (C^1), 124.3 (C^4), 124.5, 126.1 (C^5), 127.7 (C^2/C^3), 128.0 (C^2/C^3), 128.1 (C^7), 128.3, 128.4 (C^6), 131.9 (C^8), 132.8, 135.0, 139.4, 139.9, 147.9, 152.2. ESIMS: m/z 410 $[M + H]^+$. HRMS (ES): calcd for $C_{25}H_{20}N_3O_3$ $[M + H]^+$410.1505, found 410.1502.

3cd′. ^{1}H NMR (400 MHz, $CDCl_3$): δ 3.32 (t, J = 5.5 Hz, 2H, CH_2CH_2OH), 4.02 (q, J = 5.5 Hz, 2H,CH_2CH_2OH), 4.16 (t, J = 5.5 Hz, 1H, O*H*), 7.09 (d, J = 7.8 Hz, 1H, H^4), 7.42 (s, 1H, *Pz-H*), 7.41−7.51 (m, 4H, H^3, H^6, H^7), 7.56−7.61 (m, 1H, H^2), 7.57 (dd, J = 6.7, 9.0 Hz, 2H, H^8), 8.02 (dd, J = 1.6, 7.0 Hz, 2H, H^5), 8.21 (d, J = 8.2 Hz, 1H, H^1), 8.41 (dd, J = 6.7, 8.6 Hz, 2H, H^9). ^{13}C {^{1}H} NMR (100 MHz, $CDCl_3$): δ 31.6 (CH_2CH_2OH), 61.0 (CH_2CH_2OH), 94.3 (Pz), 120.9, 122.3, 122.8 (C^1), 123.0 (C^9), 124.8 (C^4), 125.4 (C^5), 126.5 (Ar), 127.3 (Ar), 127.7 (Ar), 127.9 (C^6), 128.1, 131.2 (C^8), 131.6, 134.3, 139.0, 142.6, 146.7, 151.7. ESIMS: m/z 410 $[M + H]^+$. HRMS (ES): calcd for $C_{25}H_{20}N_3O_3$ $[M + H]^+$410.1505, found 410.1494.

dx.doi.org/10.1021/jo402592z | J. Org. Chem. 2014, 79, 1954−1970

Synthesis of 3dd and 3dd′. Following the general procedure, a Schlenk flask was loaded with $[Rh(MeCN)_3Cp^*][PF_6]_2$ (16 mg, 5 mol %), 3-phenyl-5-(trifluoromethyl)-1*H*-pyrazole (**1d**, 212 mg, 1.0 mmol), $Cu(OAc)_2{\cdot}H_2O$ (500 mg, 2.5 mmol), **2d**, 4-(nitrophenyl)-but-3-yn-1-ol (115 mg, 0.6 mmol), and DCE (5 mL). The crude ^1H NMR spectrum showed the presence of two products in a 1:1 ratio. The products were purified by column chromatography eluting from 10% ethyl acetate in dichloromethane to give and **3dd** and **3dd′** (163 mg, 90% combined yield, 0.45 mmol). Compound **3dd′** was obtained as an orange solid (18 mg, 9%, 0.05 mmol) and **3dd** as an orange solid (impure).

3dd′. ^1H NMR (400 MHz, $CDCl_3$): δ 2.40 (br s, 1H, O*H*), 3.28 (t, J = 5.9 Hz, 2H, CH_2CH$_2$OH), 4.02 (br q, J = 5.9 Hz, 2H, CH$_2$CH_2OH), 7.11 (d, J = 8.2 Hz, 1H, H^4), 7.36 (s, 1H, *Pz-H*), 7.48−7.53 (m, 1H, H^3), 7.59 (dt, J = 2.3, 9.0 Hz, 2H, H^5), 7.62−7.66 (m, 1H, H^2), 8.19 (d, J = 7.8 Hz, 1H, H^1), 8.42 (dt, J = 2.3, 8.6 Hz, 2H, H^6). ^{13}C {^1H} NMR (100 MHz, $CDCl_3$): δ 32.4 (CH_2CH$_2$OH), 60.9 (CH$_2$CH$_2$OH), 96.7 (Pz), 123.3, 123.8 (C^1), 124.1 (C^6), 124.4, 126.1 (C^4), 128.2 (C^2), 129.1 (C^3), 129.2, 132.1 (C^5), 134.5, 139.5, 142.9, 148.0. ^{19}F {^1H} NMR (376 MHz, $CDCl_3$): δ −61.6 (CF_3). ESIMS: *m*/*z* 402 $[M + H]^+$. HRMS (ES): calcd for $C_{20}H_{15}N_3F_3O_3$ $[M + H]^+$402.1066, found 402.1067.

3dd. This was obtained in a mixture with **3dd′**. ^1H NMR (400 MHz, $CDCl_3$): δ 3.07 (t, J = 5.9 Hz, 2H, CH_2CH$_2$OH), 3.88 (t, J = 5.9 Hz, 2H, CH$_2$CH_2OH), 6.76 (s, 1H, *Pz-H*), 7.40−8.19 (multiplets, 7H, *Ar-H*), 8.34 (dt, J = 2.3, 8.6 Hz, 2H, *Ar-H*). ESIMS: *m*/*z* 402 $[M + H]^+$, 386 $[M - O]^+$.

Synthesis of 5da. Following the general procedure, a Schlenk flask was loaded with $[Rh(MeCN)_3Cp^*][PF_6]_2$ (33 mg, 5 mol %), 3-(thiophene-2-yl)-5-(trifluoromethyl)-1*H*-pyrazole (222 mg, 1.0 mmol), $Cu(OAc)_2{\cdot}H_2O$ (500 mg, 2.5 mmol), 4-octyne (**2a**, 132 mg, 1.2 mmol), and DCE (10 mL). The crude ^1H NMR spectrum showed the presence of two products in a 4:1 ratio. The products were purified by column chromatography eluting from 50% dichloromethane in petroleum ether (40−60 °C) to 100% dichloromethane to give **5da** as a white solid (261 mg, 79%, 0.79 mmol) (mp 79−82 °C), and a small amount of a vinyl product was also formed. Compound **5da** was also obtained with $[RuCl_2(p\text{-cymene})]_2$ as catalyst with $AgPF_6$ (25 mg, 0.1 mmol) as additive (yield 40%, based on NMR integration against an internal standard). A vinyl product was also formed.

5da. ^1H NMR (400 MHz, $CDCl_3$): δ 1.06 (t, J = 7.4 Hz, 3H, H^5), 1.07 (t, J = 7.0, 7.4 Hz, 3H, H^8), 1.65−1.74 (m, 2H, H^4), 1.76−1.85 (m, 2H, H^7), 2.89−2.93 (m, 2H, H^3), 3.22−3.26 (m, 2H, H^6), 6.90 (s,1H, *Pz-H*), 7.38 (d, J = 5.5 Hz, 1H, H^2), 7.52 (d, J = 5.1 Hz, 1H, H^1). ^{13}C {^1H} NMR (100 MHz, $CDCl_3$): δ 14.2 (C^5/C^8), 14.3 (C^5/C^8), 20.8 (C^7), 24.0 (C^4), 29.4 (C^6), 31.6 (C^3), 93.8 (Pz), 120.5, 121.8 (q, J = 270.4 Hz,CF_3), 123.2 (C^2), 125.9, 126.7 (C^1), 135.7, 135.9, 136.6, 142.8 (q, J = 39.9 Hz,C-CF_3). ^{19}F {^1H} NMR (376 MHz, $CDCl_3$): δ −61.2 (CF_3). ESIMS: *m*/*z* 327 $[M + H]^+$. HRMS (ES): calcd for $C_{16}H_{18}N_2F_3S_1$ $[M + H]^+$327.1143, found 327.1158.The product was recrystallized from dichloromethane/hexane to give **5da** as clear needles.

Synthesis of 5db. Following the general procedure, a Schlenk flask was loaded with $[Rh(MeCN)_3Cp^*][PF_6]_2$ (16 mg, 5 mol %), 3-(thiophene-2-yl)-5-(trifluoromethyl)-1*H*-pyrazole (222 mg, 1.0 mmol), $Cu(OAc)_2{\cdot}H_2O$ (250 mg, 1.25 mmol), diphenylacetylene (**2b**, 214 mg, 1.2 mmol), and DCE (10 mL). The product was purified by washing with hexane to give **5db** as an orange powder (348 mg, 88%, 0.88 mmol) (mp 230−232 °C), and a vinyl byproduct was also formed. ^1H NMR (500 MHz, $CDCl_3$): δ 7.04 (s, 1H, *Pz-H*), 7.09 (d, J = 5.1 Hz, 1H, H^3), 7.19 (dd, J = 2.7, 7.0 Hz, 2H, H^3), 7.24−7.30 (m, 6H, H^4, H^5, H^7, H^8), 7.35 (dd, J = 2.7, 7.0 Hz, 2H, H^6), 7.48 (d, J = 5.5 Hz, 1H, H^1). ^{13}C {^1H} NMR (125 MHz, $CDCl_3$): δ 94.2 (Pz), 121.5 (q, J = 270.1 Hz, CF_3), 123.9, 125.3 (C^2), 126.8 (C^1), 127.0, 127.5 (C^5/C^8), 127.9 (C^4/C^7), 128.2 (C^4/C^7), 128.7 (C^5/C^8), 130.7 (C^3), 131.5 (C^6), 131.8, 135.4, 136.5, 136.6, 136.9, 143.8 (q, J = 39.7 Hz, CF_3), ^{19}F {^1H} NMR (376 MHz, $CDCl_3$): δ −61.3 (CF_3). ESIMS: *m*/*z* 395 $[M + H]^+$. HRMS (ES): calcd for $C_{22}H_{14}N_2F_3S_1$ $[M + H]^+$395.0830, found 395.0839.

Initial Rates Experiments. Reaction vials equipped with a stirrer bar were loaded with 5-methyl-3-phenyl-1*H*-pyrazole (**1a**, 52 mg, 0.33 mmol), 4-octyne (**2a**, 0.3−2.4 equiv), $Cu(OAc)_2{\cdot}H_2O$ (165 mg, 0.83 mmol, 2.5 equiv), 1,3,5-trimethoxybenzene (3.0 mg, 0.017 mmol, 5 mol %) as internal standard, and DCE (reaction made up to 5 mL volume). The vials were sealed with a screw cap and transferred to a preheated heating block at 50 °C to stir for 5 min. $[Rh(MeCN)_3Cp^*][PF_6]_2$ (11 mg, 0.017 mmol, 5 mol %) was added, and timing was started. Each reaction was repeated to calculate the average rate. After a suitable time, a vial was removed and placed in an ice bath to stop the reaction. The mixture from each vial was diluted with diethyl ether (10 mL), and 2 M ammonium solution (10 mL) was added. The blue aqueous layer was extracted with diethyl ether (3 × 10 mL), and the combined organic layers were dried over $MgSO_4$. The solvent was removed on the rotary evaporator. The ^1H NMR spectra were recorded, and yield was found by integrating the CH_2 2H peak of the product. The order in alkyne was found to be 0.07 ± 0.1.

A similar procedure was used with $[RuCl_2(p\text{-cymene})]_2$ as catalyst, except the reactions were carried out a smaller scale, in *tert*-amyl alcohol at 100 °C. The amounts used were 5-methyl-3-phenyl-1*H*-pyrazole (**1a**, 32 mg, 0.20 mmol), 4-octyne (**2a**, 0.3−2.4 equiv), $Cu(OAc)_2{\cdot}H_2O$ (100 mg, 0.50 mmol, 2.5 equiv), 1,3,5-trimethoxybenzene (1.7 mg, 0.010 mmol, 5 mol %) as internal standard, and *tert*-amyl alcohol (reaction made up to 5 mL volume). The vials were sealed with a screw cap and transferred to a preheated heating block at 100 °C to stir for 5 min. $[RuCl_2(p\text{-cymene})]_2$ (6.1 mg, 0.01 mmol, 5 mol %) was added, and timing was started. The reactions were worked up as for Rh above.

KIE Experiment with Rh. The same general procedure as above was followed using 5-methyl-3-phenyl-1*H*-pyrazole (**1a**, 52 mg, 0.33 mmol) and **d^3-1a** (53 mg, 0.33 mmol) with 4-octyne (**2a**, 44 mg, 0.39 mmol, 1.2 equiv), $Cu(OAc)_2{\cdot}H_2O$ (165 mg, 0.83 mmol, 2.5 equiv), and the catalyst (5 mol % $[Rh(MeCN)_3Cp^*][PF_6]_2$) 1,3,5-trimethoxybenzene (3.0 mg, 0.017 mmol, 5 mol %) as internal standard, and DCE (reaction made up to 5 mL volume). Each reaction was done twice. The ^1H NMR spectra were recorded, and yield was found by integrating the CH_2 2H peak of the product. After rates for each reaction were calculated, the kinetic isotope effects were calculated as k_H/k_D = 2.7 ± 0.5 for Rh. A similar procedure was followed for Ru and k_H/k_D = 1.1 ± 0.2 for Ru.

KIE Experiment with Ru. The general procedure for the initial rates experiment was followed using 5-methyl-3-phenyl-1*H*-pyrazole (**1a**, 32 mg, 0.20 mmol) and **d^3-1a** (32 mg, 0.20 mmol) with 4-octyne (**2a**, 26 mg, 0.24 mmol, 1.2 equiv), $Cu(OAc)_2{\cdot}H_2O$ (100 mg, 0.50 mmol, 2.5 equiv), 1,3,5-trimethoxybenzene (1.7 mg, 0.01 mmol, 5 mol %), and DCE (reaction made up to 3 mL volume). The vials were sealed with a screw cap and transferred to a preheated heating block at 83 °C to stir for 5 min. $[RuCl_2(p\text{-cymene})]_2$ (6.1 mg, 0.01 mmol, 5 mol %) was added, and timing was started. All reactions were left on for 60 min. Each reaction had a repeat reaction within the same heating block in order to calculate averages. The ^1H NMR spectra were recorded and yield was found by integrating the CH_2 2H peak of the product. This led to a k_H/k_D = 1.1 ± 0.2.

General Procedure for Deuteration of Pyrazoles. A Schlenk flask equipped with a stirrer bar was evacuated and backfilled with nitrogen. It was loaded with the relevant pyrazole (1.0 mmol), the relevant metal catalyst (0.05 equiv of metal), NaOAc (164 mg, 2.0 mmol, 2 equiv), and CD_3OD (2.5 mL). The flask was sealed with a screw cap and transferred to a preheated oil bath at 60 °C to stir overnight. Monitoring by ^1H NMR showed some deuteration had occurred. PivOD (16 mg, 0.2 mmol, 0.2 equiv) was added, and the reaction was stirred at 60 °C with further monitoring. Changing the CD_3OD on one or two occasions led to high (>97%) deuterium incorporation.

Deuteration in the Presence of Alkyne. Following the general procedures for catalysis reactions (see above), a Schlenk flask was loaded with $[Rh(MeCN)_3Cp^*][PF_6]_2$ (16 mg, 5 mol %), 3-phenyl-5-methyl-1*H*-pyrazole (**1a**, 79 mg, 0.50 mmol), $Cu(OAc)_2{\cdot}H_2O$ (250 mg, 1.25 mmol), 4-octyne (66 mg, 0.60 mmol), and CD_3OD (3 mL) and transferred to a preheated oil bath at 70 °C. After 16 h, this gave

dx.doi.org/10.1021/jo402592z | J. Org. Chem. 2014, 79, 1954−1970

d²-3aa as a brown solid (124 mg, 93%, 0.47 mmol). Reaction on the same scale with the catalyst $[RuCl_2(p\text{-cymene})]_2$ (15 mg, 0.025 mmol, 2.5 mol %) gave after 16 h **d¹-3aa** as a brown solid (130 mg, 97%, 0.49 mmol).

X-ray Crystal Structure Determination of 3ac, 3dc, 3da, 5da, and 3db. Data were collected on a Bruker Apex 2000 CCD diffractometer using graphite-monochromated Mo Kα radiation, λ = 0.7107 Å. The data were corrected for Lorentz and polarization effects, and empirical absorption corrections were applied. The structure was solved by direct methods and with structure refinement on F^2 employed in SHELXTL version 6.10.[39] Hydrogen atoms were included in calculated positions (C−H = 0.93−1.00 Å, O−H = 0.84 Å) riding on the bonded atom with isotropic displacement parameters set to $1.5U_{eq}$ (O) for hydroxyl H atoms, $1.5U_{eq}$ (C) for methyl hydrogen atoms and $1.2U_{eq}$ (C) for all other H atoms. All non-hydrogen atoms were refined with anisotropic displacement parameters without positional restraints. Disordered solvent was removed with the Squeeze option in PLATON.[40] Figures were drawn using the program ORTEP.[41] Coordinates have been deposited with the Cambridge crystallographic database CCDC nos. CCDC950944−950948.

Crystal Data for the Complexes. 3ac: $C_{19}H_{19}N_2O_{1.5}$, M = 299.36, tetragonal, a = 22.783(3) Å, b = 22.783(3) Å, c = 5.7864(11) Å, $\alpha = \beta = \gamma = 90°$, V = 3003.5(8) Å^3, T = 150(2) K, space group $I\bar{4}$, Z = 8, 10897 reflections measured, 2623 independent reflections (R_{int} = 0.0682). The final R1 values were 0.0597 ($I > 2\sigma(I)$), 0.0699 (all data). The final wR(F2) values were 0.1485 ($I > 2\sigma(I)$), 0.1522 (all data). GOF = 1.103.

3da: $C_{18}H_{19}F_3N_2$, M = 320.35, triclinic, a = 16.927(16) Å, b = 4.693(5) Å, c = 21.28(2) Å, $\alpha = 90°$, $\beta = 110.54(2)°$, $\gamma = 90°$, V = 1583(3) Å^3, T = 150(2) K, space group $P2(1)/n$, Z = 4, 10780 reflections measured, 2788 independent reflections (R_{int} = 0.2392). The final R1 values were 0.0722 ($I > 2\sigma(I)$) 0.2318 (all data). The final wR(F2) values were 0.1216 ($I > 2\sigma(I)$), 0.1655 (all data). GOF = 0.782.

3db: $C_{24}H_{15}F_3N_2 \cdot C_2H_3N$, M = 429.43, triclinic, a = 9.5265(15) Å, b = 9.5816(15) Å, c = 12.880(2) Å, $\alpha = 70.575(3)°$, $\beta = 70.337(4)°$, $\gamma = 84.964(3)°$, V = 1043.7(3) Å^3, T = 150(2) K, space group P-1, Z = 2, 7678 reflections measured, 3671 independent reflections (R_{int} = 0.0990). The final R1 values were 0.0723 ($I > 2\sigma(I)$) 0.1219 (all data). The final wR(F2) values were 0.1530 ($I > 2\sigma(I)$), 0.1780 (all data). GOF = 0.896.

3dc: $C_{19}H_{13}F_3N_2$, M = 326.31, monoclinic, a = 10.826(4) Å, b = 16.541(7) Å, c = 17.451(7) Å, $\alpha = 90°$, $\beta = 96.945(9)°$, $\gamma = 90°$, V = 3102(2) Å^3, T = 150(2) K, space group $P2(1)/n$, Z = 8, 22238 reflections measured, 5462 independent reflections (R_{int} = 0.1020). The final R1 values were 0.0511 ($I > 2\sigma(I)$) 0.0991 (all data). The final wR(F2) values were 0.0896 ($I > 2\sigma(I)$), 0.1027 (all data). GOF = 0.877.

5da: $C_{16}H_{17}F_3N_2S$, M = 326.38, triclinic, a = 8.548(2) Å, b = 9.543(2) Å, c = 19.894(5) Å, $\alpha = 88.270(5)°$, $\beta = 81.218(6)°$, $\gamma = 82.774(5)°$, V = 1591.0(7) Å^3, T = 150(2) K, space group P-1, Z = 4, 11669 reflections measured, 5558 independent reflections (R_{int} = 0.0973). The final R1 values were 0.0645 ($I > 2\sigma(I)$) 0.1188 (all data). The final wR(F2) values were 0.1217 ($I > 2\sigma(I)$), 0.1436 (all data). GOF = 0.896.

COMPUTATIONAL DETAILS

DFT calculations were run with Gaussian 03 (Revision D.01)[42] and Gaussian 09 (Revision A.02).[43] Rh and Ru centers were described with the Stuttgart RECPs and associated basis sets[44], and 6-31G** basis sets were used for all other atoms.[45] Initial BP86[46] optimizations were performed with Gaussian 03 using the 'grid=ultrafine' option, with all stationary points being fully characterized via analytical frequency calculations as either minima (all positive eigenvalues) or transition states (one negative eigenvalue). IRC calculations and subsequent geometry optimizations were used to confirm the minima linked by each transition state. Corrections for the effects of dichloroethane solvent (ε = 10.125) were run with Gaussian 09 and used the polarizable continuum model.[47] For the functional testing, the BP86-optimized geometries were reoptimised with Gaussian 09 using the above basis set combinations, with frequency calculations again used to confirm the nature of all stationary points. Single-point dispersion corrections to the BP86 results employed Grimme's D3 parameter set as implemented in Gaussian 09.[48]

ASSOCIATED CONTENT

Supporting Information

Crystallographic data (CIF), NMR spectra, details of kinetics and KIE measurements, and details of all computed structures and associated energies, as well as functional testing and full references 42 and 43. This material is available free of charge via the Internet at http://pubs.acs.org. CCDC 950944-950948 contain complete crystallographic data for this paper. These data can be obtained free of charge from The Cambridge Crystallographic Data Centre via www.ccdc.cam.ac.uk/data_request/cif.

AUTHOR INFORMATION

Corresponding Authors

*E-mail: warren.cross@ntu.ac.uk.
*E-mail: dld3@le.ac.uk.
*E-mail: s.a.macgregor@hw.ac.uk.

Present Address

[§]School of Science and Technology, Nottingham Trent University, Clifton campus, Nottingham NG11 8NS, U.K.

Notes

The authors declare no competing financial interest.

ACKNOWLEDGMENTS

This work was supported through EPSRC awards EP/J021709/1, EP/J002917/1 (D.L.D.), and EP/J021911/1 (S.A.M., C.L.M.). We also thank the University of Leicester for funding (Q.K.), the Spanish Government for a Postdoctoral Fellowship (EX2009-0398, A.G.A.), and Johnson Matthey for a loan of rhodium trichloride.

REFERENCES

(1) (a) Alberico, D.; Scott, M. E.; Lautens, M. *Chem. Rev.* **2007**, *107*, 174. (b) Lyons, T. W.; Sanford, M. S. *Chem. Rev.* **2010**, *110*, 1147. (c) Chen, X.; Engle, K. M.; Wang, D.-H.; Yu, J.-Q. *Angew. Chem., Int. Ed.* **2009**, *48*, 5094. (d) Colby, D. A.; Bergman, R. G.; Ellman, J. A. *Chem. Rev.* **2009**, *110*, 624. (e) Bellina, F.; Rossi, R. *Chem. Rev.* **2009**, *110*, 1082. (f) Ackermann, L. *Chem. Rev.* **2011**, *111*, 1315.

(2) (a) Davies, D. L.; Donald, S. M. A.; Macgregor, S. A. *J. Am. Chem. Soc.* **2005**, *127*, 13754. (b) Davies, D. L.; Donald, S. M. A.; Al-Duaij, O.; Fawcett, J.; Little, C.; Macgregor, S. A. *Organometallics* **2006**, *25*, 5976. (c) Davies, D. L.; Donald, S. M. A.; Al-Duaij, O.; Macgregor, S. A.; Polleth, M. *J. Am. Chem. Soc.* **2006**, *128*, 4210. (d) Boutadla, Y.; Davies, D. L.; Macgregor, S. A.; Poblador-Bahamonde, A. I. *Dalton Trans.* **2009**, 5820. (e) Boutadla, Y.; Davies, D. L.; Macgregor, S. A.; Poblador-Bahamonde, A. I. *Dalton Trans.* **2009**, 5887.

(3) (a) Musashi, Y.; Sakaki, S. *J. Am. Chem. Soc.* **2000**, *122*, 3867. (b) Garcia-Cuadrado, D.; Braga, A. A. C.; Maseras, F.; Echavarren, A. M. *J. Am. Chem. Soc.* **2006**, *128*, 1066. (c) Lafrance, M.; Fagnou, K. *J. Am. Chem. Soc.* **2006**, *128*, 16496. (d) Ackermann, L.; Vicente, R.; Althammer, A. *Org. Lett.* **2008**, *10*, 2299. (e) Lafrance, M.; Rowley, C. N.; Woo, T. K.; Fagnou, K. *J. Am. Chem. Soc.* **2006**, *128*, 8754. (f) Gorelsky, S. I.; Lapointe, D.; Fagnou, K. *J. Am. Chem. Soc.* **2008**, *130*, 10848.

(4) (a) Ueura, K.; Satoh, T.; Miura, M. *Org. Lett.* **2007**, *9*, 1407. (b) Ueura, K.; Satoh, T.; Miura, M. *J. Org. Chem.* **2007**, *72*, 5362. (c) Shimizu, M.; Hirano, K.; Satoh, T.; Miura, M. *J. Org. Chem.* **2009**, *74*, 3478. (d) Mochida, S.; Hirano, K.; Satoh, T.; Miura, M. *J. Org. Chem.* **2009**, *74*, 6295. (e) Fukutani, T.; Umeda, N.; Hirano, K.; Satoh,

T.; Miura, M. *Chem. Commun.* **2009**, 5141. (f) Umeda, N.; Hirano, K.; Satoh, T.; Miura, M. *J. Org. Chem.* **2009**, *74*, 7094. (g) Umeda, N.; Tsurugi, H.; Satoh, T.; Miura, M. *Angew. Chem., Int. Ed.* **2008**, *47*, 4019.
(5) (a) Stuart, D. R.; Bertrand-Laperle, M.; Burgess, K. M. N.; Fagnou, K. *J. Am. Chem. Soc.* **2008**, *130*, 16474. (b) Guimond, N.; Fagnou, K. *J. Am. Chem. Soc.* **2009**, *131*, 12050.
(6) Song, G.; Wang, F.; Li, X. *Chem. Soc. Rev.* **2012**, *41*, 3651.
(7) Arockiam, P. B.; Bruneau, C.; Dixneuf, P. H. *Chem. Rev.* **2012**, *112*, 5879.
(8) (a) Li, L.; Brennessel, W. W.; Jones, W. D. *J. Am. Chem. Soc.* **2008**, *130*, 12414. (b) Li, L.; Brennessel, W. W.; Jones, W. D. *Organometallics* **2009**, *28*, 3492. (c) Sortais, J. B.; Pannetier, N.; Holuigue, A.; Barloy, L.; Sirlin, C.; Pfeffer, M.; Kyritsakas, N. *Organometallics* **2007**, *26*, 1856. (d) Boutadla, Y.; Al-Duaij, O.; Davies, D. L.; Griffith, G. A.; Singh, K. *Organometallics* **2009**, *28*, 433. (e) Boutadla, Y.; Davies, D. L.; Al-Duaij, O.; Fawcett, J.; Jones, R. C.; Singh, K. *Dalton Trans.* **2010**, *39*, 10447. (f) Davies, D. L.; Al-Duaij, O.; Fawcett, J.; Giardiello, M.; Hilton, S. T.; Russell, D. R. *Dalton Trans.* **2003**, 4132.
(9) (a) Li, L.; Jiao, Y.; Brennessel, W. W.; Jones, W. D. *Organometallics* **2010**, *29*, 4593. (b) Han, Y.-F.; Li, H.; Hu, P.; Jin, G.-X. *Organometallics* **2011**, *30*, 905.
(10) (a) Li, B.; Feng, H. L.; Wang, N. A. C.; Ma, J. F.; Song, H. B.; Xu, S. S.; Wang, B. Q. *Chem.—Eur. J.* **2012**, *18*, 12873. (b) Wang, N.; Li, B.; Song, H.; Xu, S.; Wang, B. *Chem.—Eur. J.* **2013**, *19*, 358.
(11) Simmons, E. M.; Hartwig, J. F. *Angew. Chem., Int. Ed.* **2012**, *51*, 3066.
(12) A DFT study of Rh(III)-catalyzed oxidative Heck coupling of phenol carbamates with alkenes has recently appeared; see: Zhang, Q.; Yu, H.-Z.; Li, Y.-T.; Liu, L.; Huang, Y.; Fu, Y. *Dalton Trans.* **2013**, *42*, 4175. Very recently, a computational study of the intramolecular annulation of benzamides with tethered alkynes has been reported; see: Quiñones, N.; Seoane, A.; García-Fandiño, R.; Mascareñas, J. L.; Gulías, M. *Chem. Sci.* **2013**, *4*, 2874.
(13) Guimond, N.; Gorelsky, S. I.; Fagnou, K. *J. Am. Chem. Soc.* **2011**, *133*, 6449.
(14) Xu, L.; Zhu, Q.; Huang, G.; Cheng, B.; Xia, Y. *J. Org. Chem.* **2012**, *77*, 3017.
(15) Umeda, N.; Hirano, K.; Satoh, T.; Shibata, N.; Sato, H.; Miura, M. *J. Org. Chem.* **2011**, *76*, 13.
(16) Li, X.; Zhao, M. *J. Org. Chem.* **2011**, *76*, 8530.
(17) Ma, W.; Graczyk, K.; Ackermann, L. *Org. Lett.* **2012**, *14*, 6318.
(18) See for examples refs 4−7, 16 and 17 and references cited therein.
(19) In this reaction there was a lot of unreacted **1b**, the yield based on **1b** consumed is 98%.
(20) Clar, E. *Polycyclic Hydrocarbons*; Academic Press: London, 1964.
(21) Morimoto, K.; Hirano, K.; Satoh, T.; Miura, M. *Org. Lett.* **2010**, *12*, 2068.
(22) Wang, H.; Glorius, F. *Angew. Chem., Int. Ed.* **2012**, *51*, 7318.
(23) A similar mechanism has been proposed by Li; see ref 16.
(24) Note that in similar studies (ref 17) with nitrophenyl-substituted pyrazoles Ackermann found that CH activation was reversible and that deuterium exchange occurred even in the presence of diphenylacetylene, suggesting that the relative barriers to CH activation and alkyne insertion are substrate dependent as expected.
(25) This value is likely to arise from a combination of a kinetic isotope effect arising from the proportion of the substrate that reacts straight through to the coupled products after C−H bond activation and an equilibrium isotope effect due to the proportion of C−H activated intermediates that undergo the reverse reprotonation.
(26) All optimizations aiming to locate an equivalent planar form of **E** reverted back to boat structures such as that shown in Figure 4.
(27) Based on the free energy change associated with the reaction of 5-phenyl-3-methylpyrazole + RCCH (R = H, ^{n}Pr) to give the corresponding pyrazoloisoquinoline products + H_2. ΔG_{DCE} = −43.3 kcal/mol (R = H); ΔG_{DCE} = −28.0 kcal/mol (R = ^{n}Pr).
(28) (a) Ahlquist, M. S. G.; Norrby, P. O. *Angew. Chem., Int. Ed.* **2011**, *50*, 11794. (b) Minenkov, Y.; Occhipinti, G.; Jensen, V. R. *J. Phys. Chem. A* **2009**, *113*, 11833. (c) Ryde, U.; Mata, R. A.; Grimme, S. *Dalton Trans.* **2011**, *40*, 11176. (d) Sieffert, N.; Bühl, M. *Inorg. Chem.* **2009**, *48*, 4622. (e) Zhao, Y.; Truhlar, D. G. *Org. Lett.* **2007**, *9*, 1967.
(29) The alternative possibility of insertion into the Rh−N bond entails a TS at +22.0 kcal/mol, 8 kcal/mol above that for insertion into the Rh−C bond, and therefore is highly unlikely.
(30) This conclusion is not affected by the choice of solvent used in the calculations: in MeOH (the solvent used for the experimental H/D exchange studies), the computed energies of **TS(B−C)2** and **TS(D−E)** are +10.6 kcal/mol and +11.0 kcal./mol
(31) (a) Bennett, M. A.; Macgregor, S. A.; Wenger, E. *Helv. Chim. Acta* **2001**, *84*, 3084. (b) Edwards, A. J.; Macgregor, S. A.; Rae, A. D.; Wenger, E.; Willis, A. C. *Organometallics* **2001**, *20*, 2864. (c) Macgregor, S. A.; Wenger, E. *Organometallics* **2002**, *21*, 1278.
(32) Stationary points corresponding to **INT(A-B)** and **TS(B-C)2** were located on the electronic energy surface but the free energy of **TS(B-C)2** falls below that of **INT(A-B)** suggesting C−H activation proceeds directly from **B** to **C1** via **TS(B-C)1**.
(33) We cannot rule out the possibility that catalyst reoxidation is rate limiting as this would also be consistent with a KIE of 1.1. We note, however, that the computed barriers based on rate limiting C−H activation provide barriers that are consistent with the experimental conditions and reproduce the lower catalytic activity of the Ru system. We also repeated the KIE measurements starting with preformed [$Ru(OAc)_2$(*p*-cymene)] and obtained the same result as before, i.e., a k_H/k_D KIE of ca. 1.
(34) White, C.; Thompson, S. J.; Maitlis, P. M. *J. Chem. Soc., Dalton Trans.* **1977**, 1654.
(35) Pleier, A. K.; Glas, H.; Grosche, M.; Sirsch, P.; Thiel, W. R. *Synthesis* **2001**, 55.
(36) Texierboullet, F.; Klein, B.; Hamelin, J. *Synthesis* **1986**, 409.
(37) Guillou, S.; Bonhomme, F. J.; Ermolenko, M. S.; Janin, Y. L. *Tetrahedron* **2011**, *67*, 8451.
(38) Li, J.-H.; Liang, Y.; Xie, Y.-X. *J. Org. Chem.* **2005**, *70*, 4393.
(39) Bruker; Version 6.10 ed.; Bruker Inc., Madison, WI, 1998−2000.
(40) Vandersluis, P.; Spek, A. L. *Acta Crystallogr., Sect. A* **1990**, *46*, 194.
(41) Farrugia, L. J. *J. Appl. Crystallogr.* **1997**, *30*, 565.
(42) Frisch, M. J. Gaussian, Inc., Wallingford, CT, 2004.
(43) Frisch, M. J. Gaussian, Inc., Wallingford, CT, 2009.
(44) Andrae, D.; Häußermann, U.; Dolg, M.; Stoll, H.; Preuß, H. *Theor. Chim. Acta* **1990**, *77*, 123.
(45) (a) Hariharan, P. C.; Pople, J. A. *Theor. Chim. Acta* **1973**, *28*, 213. (b) Hehre, W. J.; Ditchfield, R.; Pople, J. A. *J. Chem. Phys.* **1972**, *56*, 2257.
(46) (a) Becke, A. D. *Phys. Rev. A* **1988**, *38*, 3098. (b) Perdew, J. P. *Phys. Rev. B* **1986**, *33*, 8822.
(47) Tomasi, J.; Mennucci, B.; Cammi, R. *Chem. Rev.* **2005**, *105*, 2999.
(48) Grimme, S.; Antony, J.; Ehrlich, S.; Krieg, H. *J. Chem. Phys.* **2010**, 132.